Quibas-Sima: a unique 1 Ma-old vertebrate succession in southern Iberian Peninsula

Pedro Piñero[a,b,*], Jordi Agustí[a,b,c], Casto Laborda[d], Mathieu Duval[e,f], Jian-xin Zhao[g], Hugues-Alexandre Blain[a,b,c], Marc Furió[h,i], César Laplana[j], Antonio Rosas[k], and Paloma Sevilla[l]

*Corresponding author, E-mail address: ppinero@iphes.cat (P. Piñero)

[a]IPHES-CERCA, Institut Català de Paleoecologia Humana i Evolució Social, Zona Educacional 4, Campus Sescelades URV (Edifici W3), 43007 Tarragona, Spain.

[b]Àrea de Prehistòria, Universitat Rovira i Virgili (URV), Avinguda de Catalunya 35, 43002 Tarragona, Spain.

[c]ICREA, Institució Catalana de Recerca i Estudis Avançats, Pg. Lluís Companys 23, 08010 Barcelona, Spain.

[d]Departamento de Geología (Unidad Asociada al IACT-CSIC), Universidad de Jaén, 23071, Linares, Spain.

[e]Centro Nacional de Investigación sobre la Evolución Humana (CENIEH), Burgos, 09002, Spain.

[f]Australian Research Centre for Human Evolution (ARCHE), Griffith University, Nathan, QLD 4111, Australia.

[g]Radiogenic Isotope Facility, School of Earth and Environmental Sciences, The University of Queensland, Brisbane, QLD 4072, Australia

[h]Serra Húnter fellow, Departament de Geologia, Universitat Autònoma de Barcelona, 08193, Bellaterra, Spain.

[i]Institut Català de Paleontologia Miquel Crusafont, Universitat Autònoma de Barcelona, Edifici ICTA-ICP, Carrer de les Columnes s/n, Campus de la UAB, 08193, Cerdanyola del Vallès, Barcelona, Spain.

[j]MAR, Museo Arqueológico Regional de la Comunidad de Madrid, Plaza de las Bernardas s/n, 28801 Alcalá de Henares, Spain.

[k]Departamento de Paleobiología, Museo Nacional de Ciencias Naturales (CSIC), José Gutiérrez Abascal 2, 28006 Madrid, Spain.

[l]Departamento de Geodinámica, Estratigrafía y Paleontología, Facultad de Ciencias Geológicas, Universidad Complutense de Madrid, Ciudad Universitaria, 28040 Madrid, Spain.

ABSTRACT

With the identification of the Jaramillo geomagnetic subchron, the late Early Pleistocene vertebrate succession of the Quibas-Sima section (Quibas karstic complex, southern Spain) represents a time span scarcely recorded in Europe. To complete the existing chronostratigraphic framework published earlier by Piñero et al. (2020), we provide here additional new information about the lithostratigraphy and micromammal succession along the sedimentary sequence. Seven lithostratigraphic units have been differentiated (QS-1 to QS-7) at Quibas-Sima, documenting an almost continuous small mammal record, including representatives of the families Soricidae, Erinaceidae, Rhinolophidae, Vespertilionidae, Arvicolidae, Muridae, Gliridae, Sciuridae, Leporidae and Ochotonidae. The small mammal association indicates that units QS-1 to QS-4 have an intermediate biostratigraphic position between the sites of Fuente Nueva 3 (ca. 1.2 Ma) and Cueva Victoria (ca. 0.9 Ma). New numerical age result from the combined U-series/ESR dating of one equid tooth from QS-3 consistently support the general chronostratigraphic framework based on magnetostratigraphy and biostratigraphic inferences by confirming a post-Olduvai age. Based on an estimation of the sedimentation rate during the Jaramillo subchron, these broad chronological constraints may be confidently refined to approx. 1.1–0.9 Ma for the whole sequence. While we acknowledge the existing uncertainty associated to this age range, it is nevertheless consistent with biostratigraphic evidence indicating that all stratigraphic units most likely do not significantly differ from a chronological point of view. Both independent proxies (biostratigraphy and the sedimentation rate) strongly suggest that the sedimentary sequence covers a relatively short time interval (<200 kyr). These results place the Quibas-Sima sequence as one of the longest and most complete pre-Jaramillo (QS-1) to Jaramillo (QS-2 to QS-5) continental vertebrate succession in Europe.

58 **Keywords**: Jaramillo subchron, Early Pleistocene, combined U-series/ESR dating,
59 biostratigraphy, micromammals.

60

1. Introduction

The Quibas site (Region of Murcia, Spain) is a karstic complex of cavities filled by sediments of Early Pleistocene age. It is located in an abandoned limestone quarry near the town of Cañada de la Leña, on the SE slope of the Sierra de Quibas (Fig. 1A). The location coordinates are 38°18′ 51″ N, 1°4′ 42″ W. Since its discovery in 1994, this paleontological outcrop has provided fossil remains of more than 80 species from the late Early Pleistocene, mainly including vertebrates but also some invertebrates (Montoya et al., 1999, 2001; Blain et al., 2014; Pérez-García et al., 2015; Piñero et al., 2015, 2020; Blain and Bailon, 2019; among others). The significance of this site lies in its chronology, great faunal diversity, and the outstanding preservation of its fossils.

The Quibas karstic complex hosts two main structures with paleontological content: a vertical shaft infill called Quibas-Sima (QS; 12 m deep and up to 2 m wide; Fig. 1B) and the sediments found in a gallery known as Quibas-Cueva (QC; up to 5 m wide, 9 m high and more than 30 m in length), both cavities being internally connected. A small additional detritic cavity called Quibas-Gruta1 with small vertebrate fossils is also part of this complex (Piñero et al., 2015, 2016).

The first stage of intervention at the Quibas complex was conducted from 1999 to 2009 and dealt with the Quibas-Cueva section. The data collected during that period gave place to several publications centred on the faunal assemblage. Thus, preliminary faunal lists were initially published in Montoya et al. (1999, 2001). Several papers dealt with the taxonomy of the macrovertebrate finds (Alba et al., 2011; Carlos-Calero et al., 2006a, 2006b; Made et al., 2007; Piñero and Alberdi, 2015; Pérez-García et al., 2015). As for microvertebrates, Montoya et al. (1999, 2001) included a preliminary identification of the small mammal association from Quibas-Cueva considered as a whole, making no

difference regarding their provenance from different detritic units. More recently, Piñero et al. (2015, 2016) provided a description of the rodent assemblage from Quibas-Gruta1, and proposed a first biochronological framework and paleoenvironmental reconstruction for this site, although at that time no magnetostratigraphic data were available. Finally, the significance of the herpetofauna from Quibas-Cueva has been highlighted by Blain et al. (2014), who ascertained the latest presence of agamid lizards from western Europe, while Blain and Bailon (2019) identified a new anguid species (*Ophisaurus manchenoi*), the last representative of its genus in western Europe.

However, relatively little attention has been paid to Quibas-Sima in comparison with the other sites of the karstic complex. Given the undeniable significance of the fossil record to better characterise the late Early Pleistocene faunal changes in southern Europe, new digging campaigns were restarted in this locality in 2014, with the purpose of establishing the sequence of faunal and climatic events recorded at this section. For this purpose, a detailed differentiation and characterization of each of the sedimentary units represented in Quibas-Sima was undertaken and sampling for microfauna and magnetostratigraphic analysis of the whole sedimentary sequence was performed. Palaeomagnetic results published earlier by Piñero et al. (2020) showed that Quibas-Sima section recorded a vertical succession of reversed-normal-reversed polarity along the seven lithosratigraphic units of the sedimentary infill (Fig. 1B). Specifically, the lowermost unit QS-1 provided a reverse polarity, while the intermediate units QS-2 to QS-5 were included in a normal polarity interval, and the uppermost units QS-6 and QS-7 correspond to a second reversed interval (Piñero et al., 2020). Using on biostratigraphic evidence derived from the small and large mammal assemblage, the local magnetostratigraphic section was correlated to the Global Geomagnetic Time Scale (GPTS) and the intermediate interval of normal polarity was assigned to the Jaramillo subchron (1.07–0.99 Ma; Gradstein et al., 2012).

To sum up, the Quibas-Sima section offers an excellent opportunity to thoroughly investigate the climatic and faunal events that occurred at the Early to Middle Pleistocene transition. In particular, the detailed study of the taxa present in the successive units of the Quibas-Sima section is essential for the development of a robust biostratigaphic scheme of the Pleistocene continental record in western Europe.

Consequently, in order to obtain significant results, a great effort was placed in the recent excavation campaigns to recover a large and representative number of small vertebrate remains besides the more conspicuous large vertebrates found in the site, providing an unprecedented continuous record with independent age control. This effort has proved to be worthwhile, as evidenced by the recent description of a new arvicolid genus, *Manchenomys*, of remarkable biostratigraphic value (Agustí et al., in press). Completing the preliminary description of the micromammal assemblage published earlier by Piñero et al. (2020), we provide here new and more detailed information for each of the small mammal taxa identified at Quibas-Sima, enabling thorough correlations with other Early Pleistocene localities in the Iberian Peninsula.

This paper aims to further refine the chronostratigraphy of the Quibas-Sima section, by providing a new and detailed description of the lithostratigraphy and of the small mammals, while a combined U-series and ESR dating attempt yields the first numerical age constraints for the site. Finally, a first age-depth model is proposed.

2. Geological setting

2.1. Quibas karstic complex

The Sierra de Quibas is a 6-km-long and 2.5-km-wide (~8.5 km²) calcareous massif, mainly composed of Jurassic limestones and dolostones. It runs in a NE-SW direction in

the Middle Subbetic region (Rodríguez-Estrella et al., 2004). This calcareous massif underwent intensive karstification during the Plio-Pleistocene, resulting in a variety of karstic structures along the massif. Some of these are infilled by mixed detritic sediments and/or chemical precipitates, as exemplified by the Quibas karstic complex (Durán et al., 2004). This one is composed of several different types of cavities (cave, shaft and small-sized fissures), most of which are infilled with Pleistocene sediments rich in fossil remains (namely, Quibas-Sima, Quibas-Cueva, Quibas-Gruta1; see fig. 1 in Piñero et al., 2015). These sediments consist of limestone breccia typical of cave entrances derived from a mixed source: the collapse and fragmentation of the cave roof, and the sediments of the outer slope (Piñero et al., 2020). The stratigraphic and sedimentological features of the lower part of Quibas-Cueva are described in Montoya et al. (1999), and those of the small cavity Quibas-Gruta1 in Piñero et al. (2015). A preliminary description of the geological characteristics and fossil content of Quibas-Sima is available in Piñero et al (2020).

2.2. Lithostratigraphy of Quibas-Sima locality

The roof of the Quibas-Sima structure is covered by large speleothems. Limestone and large gravel and boulders usually show longitudinal grain size sorting increasing from Quibas-Sima to Quibas-Cueva. This longitudinal sorting of the boulder and gravels points out to forms and sedimentary process of talus slope and cone deposits.

The Quibas-Sima lithostratigraphic succession is formed by seven differenciated detritic units according to sedimentological criteria, named QS-1 to QS-7 from base to top, including some thin speleothem horizons (see Fig. 1B). QS-5 and QS-6 are palaeontologically sterile units except for gastropods, while the remaining units have yielded vertebrate remains.

157 The lowermost unit, QS-1, is ~3 m thick and is subdivided from the base to the top into
158 three subunits of variable thickness: QS-1.1 (~1.8 m), QS-1.2 (~0.3 m) and QS-1.3 (~1
159 m). QS-1.1 consists of massive muddy sands of light red-brown color with fine gravel
160 clasts, granules and small speleothem clasts. Small vertebrate remains are abundant,
161 especially in some organic-matter-rich bedsets. QS-1.2 is formed by light-reddish
162 cemented sandy sediment rich in clays. It has yielded both fragmented bones of large
163 mammals and microvertebrates. QS-1.3 consists of microstratified light-brown
164 moderately cemented sand with clay fraction. Bioturbation, scours and desiccation
165 structures are observable. This subunit is rich in microfaunal remains, and has delivered
166 some large mammal bones. In its uppermost part there are two speleothem layers (Fig.
167 1B), the lower with a laminar structure, and the upper is thicker and consists of different
168 consecutive types of speleothems within the same bedset (from bottom to top): laminar,
169 coralloid and massive.

170 QS-2 unit is 1.7 m thick. In the first few centimetres, the sediments of this unit resemble
171 those of QS-1.3. The successive bedsets consist of microbreccia gravels and breccias with
172 alternation between normal and inverse grading with brown muddy sand matrix that hosts
173 some outsize large clast boulders. In the upper bedset, there are some levels of clast-
174 supported coarse-grained breccia with matrix-free voids between the clasts. This unit is
175 rich in large and small vertebrates.

176 QS-3 is a 1-m thick breccia deposit that contains boulders and gravels with reddish light-
177 yellow muddy sand matrix. Microvertebrate and macrovertebrate fossils are also
178 abundant.

179 QS-4 is a 1-m thick breccia deposit made of unimodal gravel and cemented muddy sand
180 of reddish yellow color. The lower surface boundary contains a scoured surface infilled

with boulders. The breccia deposit presents a discontinuous fine strata showing alternation between normal and inverse grading. The upper bedset is made of fine and cemented beds. The upper surface boundary of QS-4 contains a speleothem deposit and a scour with a boulder deposit of speleothems. This unit has yielded both small and large vertebrate fossils.

QS-5 unit consists of 1-m thick breccia. This deposit contains three horizontal and parallel bedsets and two lenticular bedsets close to the upper surface boundary. The lower horizontal bedsets are made of unimodal fine gravels (4-6 cm) in either clast support structure with planar fabric, or in pale brown muddy sand matrix support structure. The upper lenticular gravel beds show also alternating normal and inverse grading in open work and partly clast support structure. This unit yielded no fossils other than gastropods.

QS-6 unit is a 1-m thick breccia. This breccia is stratified in four bedsets of discontinuous and horizontal strata that contain boulders of roughly 25 cm. The breccia deposits consist of muddy sand matrix support of pale brown color with alternating normal and inverse grading (weakly developed). There are gastropod remains, but vertebrates are absent.

The poorly stratified QS-7 is a cemented breccia with a thickness of 2.5 m, and bimodal grain size distribution. It is made of medium and fine-sized gravel with limestone and speleothem clasts. This unit has a clast-supported structure infilled with calcareous pale brown muddy sands. There are two strata of large boulders made of speleothems. This unit has yielded scarce remains of small vertebrates.

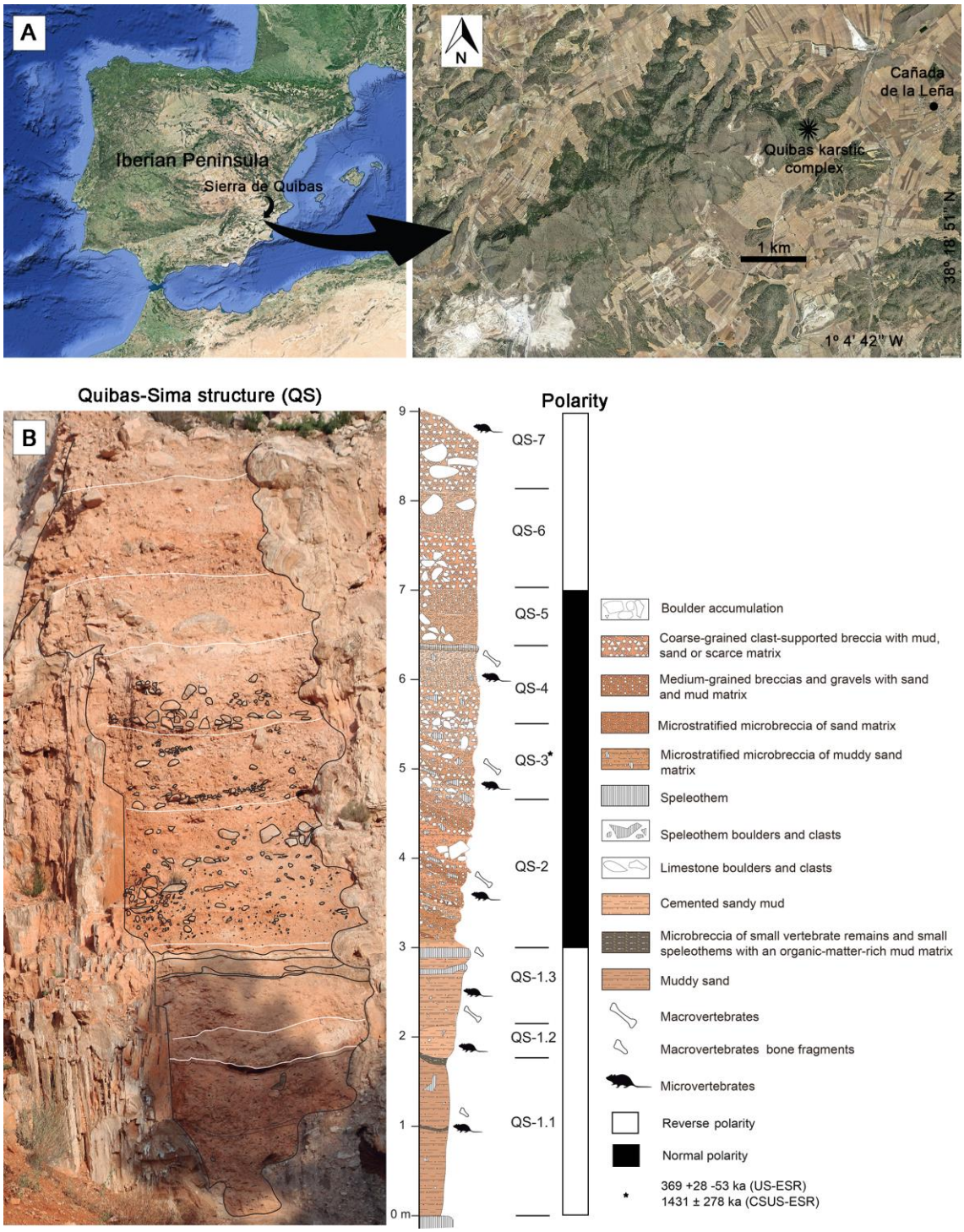

Figure 1. Geographic and stratigraphic context of the Quibas site. (A) Geographic location of the Quibas karstic complex (source Google Earth Pro). (B) Field image of the infill of Quibas-Sima, stratigraphic column and magnetostratigraphy of the section (modified from Piñero et al., 2020). Numerical age results obtained on one fossil tooth from QS-3 are indicated. [planned for 2 columns]

3. Materials and methods

3.1. Small mammal assemblage

Most of the small mammal material referred to here was collected from the Quibas-Sima section during the 2014 sampling campaign, in addition to the material recovered during the following systematic excavation campaigns (2015, 2016, 2017 and 2018). Bags of raw sediment retrieved on site were systematically water-screened using superimposed 4, 1 and 0.5 mm mesh sieves. The resulting Quibas-Sima small mammal collection includes 1134 identified remains, mainly teeth, mandibles and maxillae corresponding to 16 different micromammal taxa in total. QS-1.1 has yielded 22 specimens ascribed to eight taxa, the sample of QS-1.2 consists of 373 specimens comprising 14 taxa, the material from QS-1.3 contains 592 small mammal fossils of at least nine species, the sample from QS-2 comprises 35 remains assigned to nine taxa, QS-3 has yielded 80 remains representing 11 species, the material from QS-4 consist of 28 identified remains belonging to nine micromammal species, and QS-7 is the poorest level with only four specimens representing two species. These fossils are currently housed at the *Institut de Paleoecologia Humana i Evolució Social* (IPHES-CERCA; Tarragona, Spain), and final deposit is going to be at the *Museo Arqueológico de Murcia* (MAM; Murcia, Spain).

Small mammal teeth are illustrated by means of micrographs taken with Environmental Scanning Electron Microscopy (ESEM) at the *Servei de Recursos Científics i Tècnics de la Universitat Rovira i Virgili* (Tarragona). The upper teeth are denoted by capital letters and the lower teeth by lowercase letters. All the measurements are expressed in millimetres and were taken on the occlusal plane of the molars with the software DinoCapture 2.0, using photographs from the Digital Microscope AM4115TL Dino-Lite Edge. The nomenclature and measuring methods used in the description of murid molars

231 are those defined by van de Weerd (1976) and Martín-Suárez and Freudenthal (1993),
232 respectively. For the nomenclature and measurements of the Sciuridae, we have followed
233 Sinitsa and Pogodina (2019) and van de Weerd (1976), respectively. The terminology and
234 measuring methods employed in the descriptions of the arvicolid teeth (only m1 and M3
235 have been considered) are those of Meulen (1973), modified by Agustí et al. (in press)
236 for width of M3. Daams (1981) was followed when we describe glirids teeth, and length
237 and width have been measured as defined by Freudenthal (2004). The terminology and
238 measurements used to describe prolagid remains follow Angelone and Sesé (2009). In
239 describing and measuring the leporid teeth, we have followed the nomenclature and
240 methods proposed by López-Martínez et al. (2007). We used the terminology and
241 methods of Reumer (1984) for the Soricidae family and Mein and Furió et al. (2015) for
242 the Erinaceidae family.

243 *3.2. Combined U-series/ESR dating*

244 3.2.1. Samples

245 One fossil tooth ascribed to *Equus* cf. *altidens* (QB19-QS3-P22-5) was collected *in situ*
246 from QS-3 stratigraphic unit during the excavation campaign in 2019 for combined U-
247 series and ESR dating, together with the surrounding sediment for further laboratory
248 analyses.

249 3.2.2. Sample preparation

250 One sample (#595) was collected from the tooth and prepared following the usual ESR
251 dating procedure (e.g., Duval et al., 2019). The enamel layer was mechanically separated
252 from the other dental tissues and both inner and outer surfaces were removed with a
253 dentist drill to eliminate the volume that received an external alpha dose. The clean

enamel and dentine samples were ground and sieved <200 µm to obtain homogenous powders.

3.2.3. ESR dose evaluation

The ESR dose evaluation was performed at the *Centro Nacional de Investigación sobre la Evolución Humana* (CENIEH), Spain. Dose evaluation utilised the multiple aliquot additive dose (MAAD) method. The enamel powder from each tooth was divided into 11 aliquots and irradiated with a Gammacell 1000 Cs-137 gamma source (dose rate = 6.13 ± 0.14 Gy/min) to the following doses: 0, 49.4, 98.9, 148.3, 197.6, 296.4, 395.3, 592.9, 889.5, 1482.4 and 2964.7 Gy.

ESR measurements were carried out at room temperature with an EMXmicro 6/1 Bruker ESR spectrometer coupled to a standard rectangular ER 4102ST cavity. The following procedure was used to minimise the analytical uncertainties on the measurements: (i) all aliquots of a given sample were carefully weighted into their corresponding tubes and a variation of <1 mg was tolerated between aliquots; (ii) ESR measurements were performed using a Teflon sample tube holder inserted from the bottom of the cavity to ensure that the vertical position of the tubes remains exactly the same for all aliquots. The following acquisition parameters were used: 1 scan, 1 mW microwave power, 1024 points resolution, 15 mT sweep width, 100 kHz modulation frequency, 0.1 mT modulation amplitude, 20 ms conversion time and 5 ms time constant. All aliquots (average weight of 20.1 ± 0.2 mg per aliquot) were measured within a short time interval (<1 h). This procedure was repeated three times over successive days without removing the enamel from the ESR tubes between measurements in order to evaluate measurement and equivalent dose (D_E) precisions.

277 The ESR intensities were extracted from T1-B2 peak-to-peak amplitudes of the ESR
278 signal (Grün, 2000a) after a cubic baseline correction, and then normalised to the
279 corresponding number of scans and aliquot mass. D_E values were obtained by fitting a
280 single saturating exponential (SSE) through the mean ESR intensities derived from the
281 repeated measurements. Fitting was performed with Microcal OriginPro 9.1 software,
282 which is based on a Levenberg-Marquardt algorithm by chi-square minimisation. Data
283 were weighted by the inverse of the squared ESR intensity ($1/I^2$) (Grün and Brumby,
284 1994). The ESR dose response curve (DRC) is displayed in Fig. 2, while numerical fitting
285 results are given in Table 1.

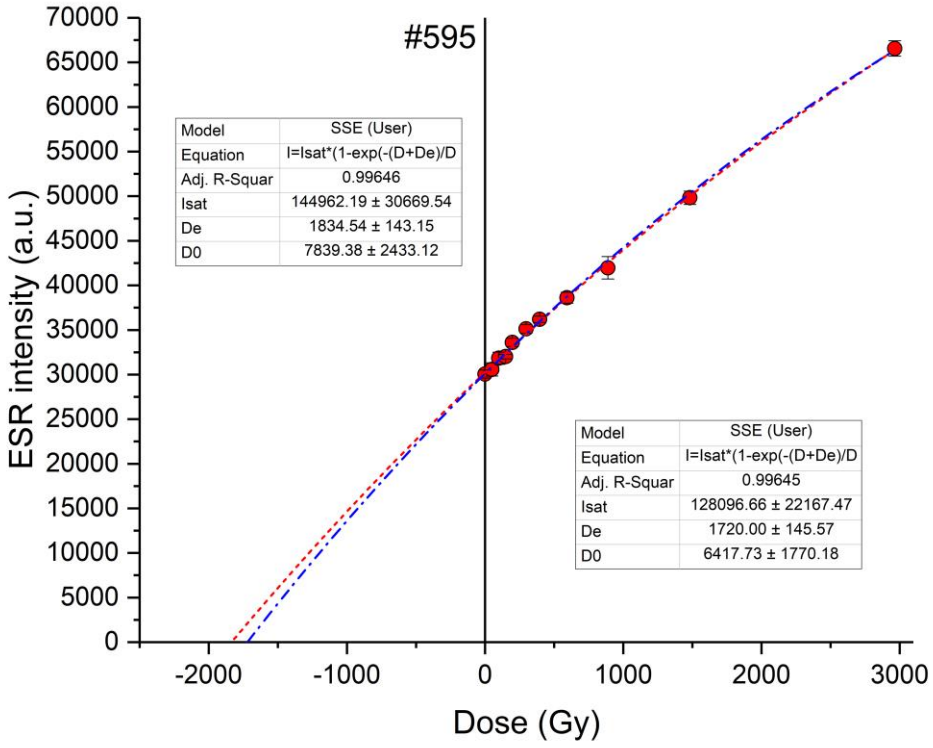

286

287 **Figure 2**. ESR dose response curve obtained for sample #595. Fitting was performed with
288 a SSE function using data weighting by $1/I^2$ (red line) and $1/s^2$ (blue line). [planned for 2
289 columns]

290 3.2.4. Solution U-series analyses by MC-ICPMS

291 Solution U-series analyses of powdered enamel and dentine were carried out using a Nu
292 Plasma HR MC-ICP-MS in the Radiogenic Isotope Facility (RIF) at the School of Earth
293 and Environmental Sciences, the University of Queensland (Australia), following
294 chemical treatment procedures and MC-ICP-MS analytical protocols described elsewhere
295 (e.g. Zhao et al., 2001; Clark et al., 2014). Powdered sub-samples weighing 1–5 mg were
296 spiked with a mixed ^{229}Th-^{233}U tracer and then completely dissolved in concentrated
297 HNO_3. After digestion, each sample was treated with H_2O_2 to decompose trace amounts
298 of organic matters and to facilitate complete sample-tracer homogenisation. U and Th
299 were separated using conventional anion-exchange column chemistry using Bio-Rad AG
300 1-X8 resin. After stripping off the matrix from the column using double-distilled 7N
301 HNO_3 as eluent, 3 ml of a 2% HNO_3 solution mixed with trace amount of HF was used
302 to elute both U and Th into a 3.5-ml pre-cleaned test tube. After column chemistry, the
303 U-Th mixed solution was injected into the MC-ICP-MS through a DSN-100 desolvation
304 nebuliser system with an uptake rate of around 0.07 ml per minute. U-Th isotopic ratio
305 measurement was performed on the MC-ICP-MS using a detector configuration to allow
306 simultaneous measurements of both U and Th. Closed-system U-series ages were
307 calculated using the Isoplot/Ex 3.75 Program (Ludwig, 2012). Analytical results are given
308 in Table 2.

309 3.2.5. Age calculations

310 U, Th and K contents were obtained from the ICP-OES/MS analysis of the dry raw
311 sediment (previously powdered and homogenized) following a four-acid digest
312 preparation procedure. Data are given in Table 2. These values were used to derive the
313 beta and gamma dose rate for the tooth. The following parameters were used for the dose
314 rate calculations: an alpha efficiency of 0.13 ± 0.02 (Grün and Katzenberger-Apel, 1994),

315 Monte-Carlo beta attenuation factors from Marsh (1999), dose-rate conversion factors
316 from Guérin et al. (2011), an estimated water content of 0 and 5 ± 3 wt.% in enamel and
317 dentine, respectively. A long-term water content value of 20 ± 5% (percentage wet
318 weight) was employed for the age calculation. A large absolute error of 5% (1σ) was
319 assumed on the long-term water content in order to cover major humidity fluctuations
320 over time. Cosmic dose rate was calculated using Prescott and Hutton (1994), using an
321 estimated depth of 4 m and an overall density of 2.5 g/cm^3 for the overburden. Finally, a
322 geometry sediment/enamel/dentine was considered for the beta dose rate calculation.

323 Age calculations were performed with DATA, a DOS-based program (Grün, 2009), and
324 using the US and CSUS models defined by Grün et al. (1988) and Grün (2000b),
325 respectively. Data inputs and outputs are given in Table 2.

326 **4. Small mammal succession**

327 The small mammal succession from the Quibas-Sima section (Fig. 3) comprises
328 insectivores (Soricidae, Erinaceidae), bats (Rhinolophidae, Vespertilionidae), rodents
329 (Arvicolidae, Muridae, Gliridae, Sciuridae) and lagomorphs (Leporidae, Ochotonidae).

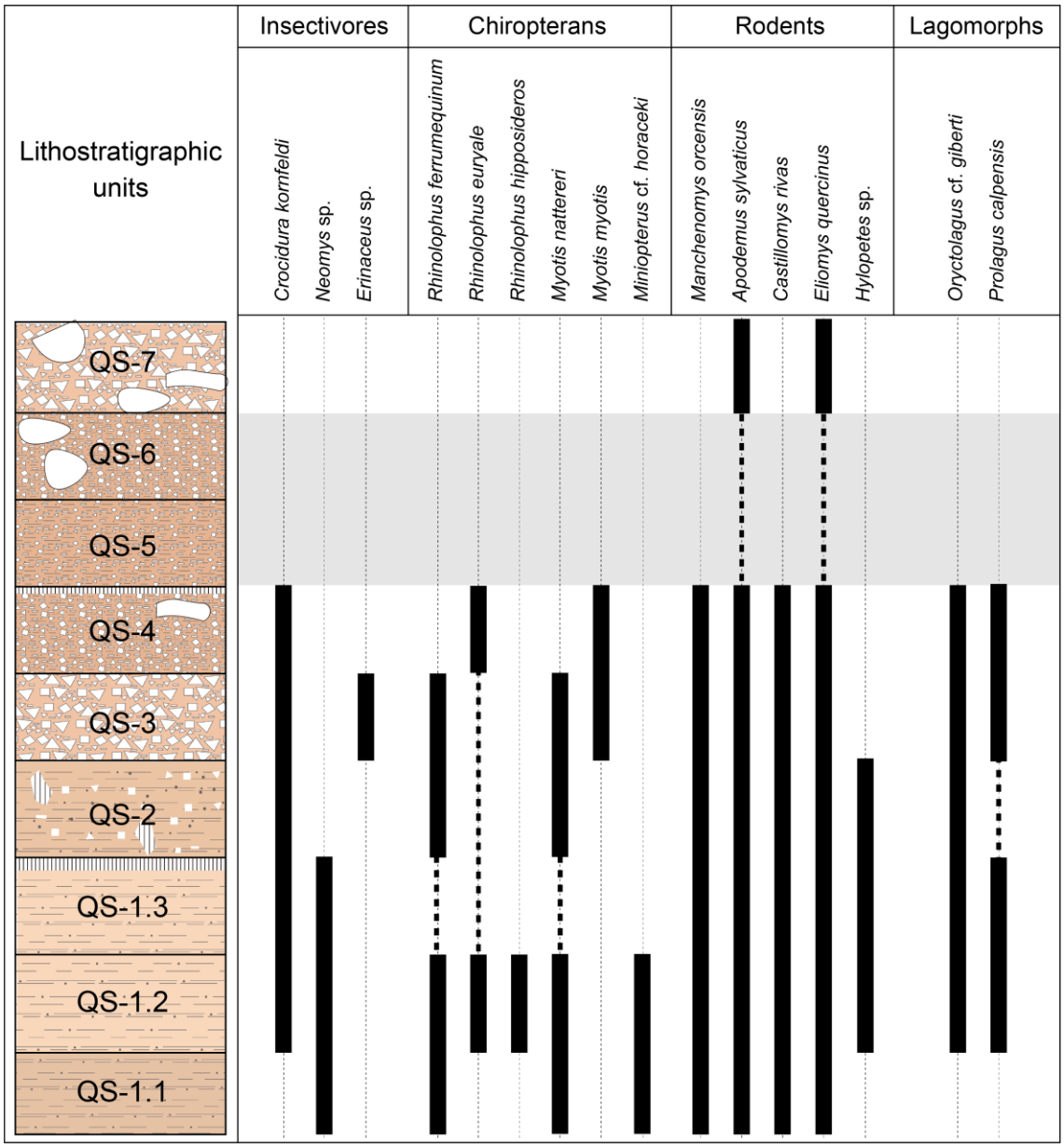

Figure 3. Distribution chart of the small mammal taxa found in the Quibas-Sima section. [planned for 2 columns]

Order SORICOMORPHA Gregory, 1910

Family Soricidae Fischer, 1817

Genus *Neomys* Kaup, 1829

Neomys sp.

337 The species *Neomys* sp. has been recorded in the levels QS-1.1 (one molar), QS-1.2 (five
338 molars and one mandible) and QS-1.3 (one molar) (Fig. 4C, D) (see dimensions in Table
339 S1). The structure of the condyle, with two clearly separated facets and a long and narrow
340 interarticular area, leaves no doubt on the ascription of this material to a species of
341 Neomyini. Only two genera of Neomyini, *Asoriculus* and *Neomys*, are known to occur in
342 the late Early Pleistocene of the Iberian Peninsula (Furió et al., 2018). The rather faint
343 construction of the teeth, without strong basal cingula or inflated cuspids, indicates that
344 these remains belong to *Neomys*. The identification of the species is somewhat more
345 difficult for two reasons. First, because a taxonomic revision of the fossil record of this
346 genus is yet to be done, especially for the Early and Middle Pleistocene material. Second,
347 because the material of *Neomys* in Quibas-Sima is really scanty, and some specific
348 diagnostic elements are missing. The latest contributions to the group (Rzebik-Kowalska,
349 2013; Botka and Mészáros, 2017) found that *Neomys newtoni* was present in similarly-
350 aged assemblages. However, the material from Quibas-Sima does not show all the
351 specific traits of this form.

352 The presence of *Neomys* in the Iberian small mammal assemblages becomes rather
353 frequent close to the transition from the Early to early Middle Pleistocene (Furió et al.,
354 2018). So far, the oldest known occurrences of *Neomys* in the Iberian Peninsula
355 correspond to the late Early Pleistocene sites of Almenara-Casablanca 3 (Agustí et al.,
356 2011) and Gran Dolina TD3–TD8 (Cuenca-Bescós et al., 2015). In the somewhat older
357 sites like Sima del Elefante TE7–TE14, and Orce (Fuente Nueva 3 and Barranco León 5)
358 the Neomyini present is *Asoriculus gibberodon* (Rofes and Cuenca-Bescós, 2006; Agustí
359 et al., 2010, 2015a; Cuenca-Bescós et al., 2015; Furió, 2007). This is why the faunal list
360 from Quibas provided by Montoya et al. (2001) quoting the presence of *Neomys* had been
361 questioned in Furió (2007) as a likely confusion with remains of *A. gibberodon*. However,

362 the direct evaluation of the material now confirms the real presence of *Neomys* in the
363 levels QS-1.1, QS-1.2 and QS-1.3 from Quibas, instead of such hypothetical occurrence
364 of *Asoriculus*. Therefore, the occurrence of *Neomys* in Quibas-Sima is probably the oldest
365 record of this genus in Spain known up to date.

366 *Crocidura kornfeldi* Kormos, 1934

367 The soricid *Crocidura kornfeldi* is almost invariably present in all the levels, represented
368 by three molars in QS-1.2, four mandibles and a total of 24 teeth in QS-1.3, one mandible
369 in QS-2, four mandibles and a total of 10 teeth in QS-3, and one mandible in QS-4 (Fig.
370 4A, B) (measurements are shown in Table S2). Its lack of record in QS-1.1 and QS-7 is
371 more likely a result of a sampling bias rather than a real absence. The genus *Crocidura*
372 arrived to the Iberian Peninsula at about 1.5 Ma, and it becomes a rather frequent element
373 in the latest Early Pleistocene small mammal assemblages (Furió et al., 2018). The species
374 *Crocidura kornfeldi* has been reported in other Early Pleistocene sites from Spain, such
375 as Sima del Elefante TE7–TE14 (Rofes and Cuenca-Bescós, 2011), Fuente Nueva 3 and
376 Barranco León 5 (Agustí et al., 2010, 2015a) and Cueva Victoria (Furió et al., 2015). In
377 the latest Early Pleistocene sites like Almenara-Casablanca 3 (Agustí et al., 2011) and
378 Gran Dolina TD3–TD8 (Cuenca-Bescós et al., 2015) the genus *Crocidura* is represented
379 by an undetermined species.

380 Order ERINACEOMORPHA Gregory, 1910

381 Family Erinaceidae Fischer, 1817

382 Genus *Erinaceus* Linnaeus, 1758

383 Only one molar (m2) found in QS-3 is attributable to *Erinaceus* sp. (Fig. 4E) (length: 5.03
384 mm; width: 3.40 mm). The genus *Erinaceus* is apparently present in the Iberian Peninsula

385 from the Turolian (7.5 Ma) to the present day (Furió et al., 2018), although its occurrences
386 in the fossil record are rather anecdotic and scattered in time and space. This fact is
387 possibly related with the territorial nature of its species, characterized by having only a
388 few individuals per unit of area. The fact that *Erinaceus* is usually found in the best
389 sampled paleontological sites from the Early Pleistocene of Spain is probably supporting
390 this interpretation. In the case of Quibas, the genus is only represented by one m2 from
391 the level QS-3. In the locality of Cueva Victoria (southern Spain), the insectivore
392 assemblage is limited to *Crocidura kornfeldi* and *Erinaceus* cf. *preglacialis* (Furió et al.,
393 2015), but the dominance of the former taxon is simply overwhelming. In the light of the
394 number of specimens of other insectivores recovered in Quibas-Sima, this single
395 erinaceid tooth represents a similar ratio between hedgehogs and shrews to that found in
396 Cueva Victoria. Thus, it cannot be ruled out that *Erinaceus* was present in the nearby area
397 during the sedimentation of all the layers, but it was not recorded simply because it was
398 a minor component of the small mammal communities.

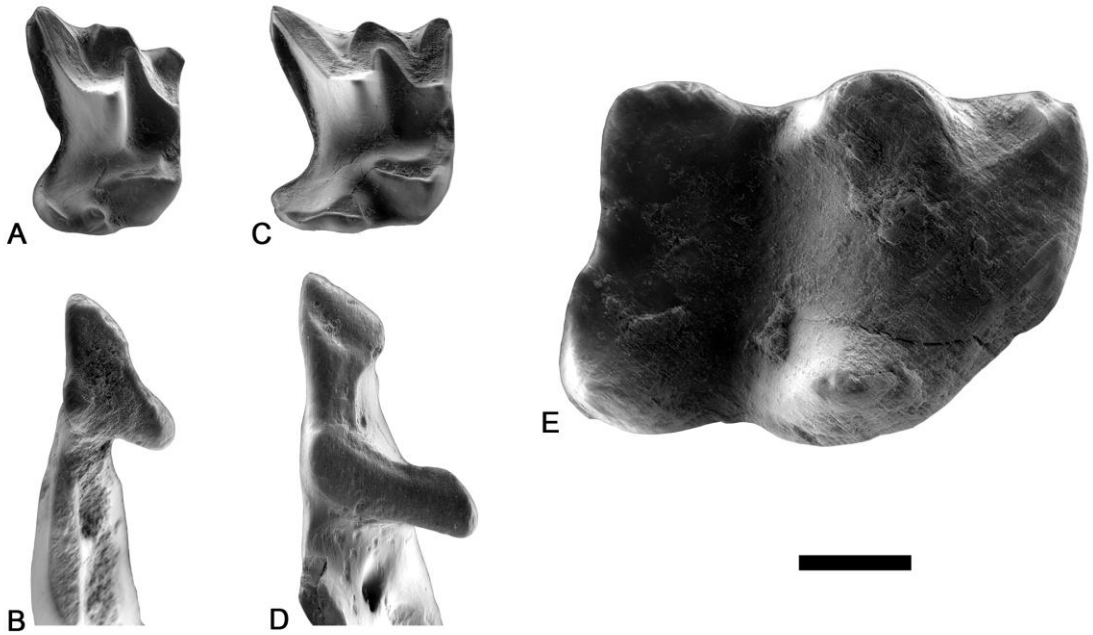

399

Figure 4. ESEM images of insectivores from Quibas-Sima. (A-B) *Crocidura kornfeldi*: A- right M1 from QS-1.3 in occlusal view (IPHES-QS1Z-I/AC2); B- articular condyle in posterior view. (C-D) *Neomys* sp.: C- right M1 from QS-1.3 in occlusal view (IPHES-QS1Z-I/AC1); D- articular condyle in posterior view. (E) *Erinaceus* sp.: right m2 from QS-3 in occlusal view (IPHES-QS3-I/AC1). Scale bar equals 1 mm. [planned for 2 columns]

Order CHIROPTERA Blumenbach, 1779

Compared to the Quibas-Cueva record (Sevilla et al., 2014), where 11 different species were identified, the bat remains from this section are so far rather scarce in number, although not so much considering species richness. Up to now, the chiropteran assemblage from Quibas-Sima comprises six species, most of them common in Quaternary sites and typically linked to karst environments (López-García et al., 2011; Sevilla and López-García, 2010). In contrast to the Quibas-Cueva record, no remains of tree-dwelling species such as *Plecotus* sp. or *Pipistrellus* sp. were found in the Quibas-Sima section, and probably most of the material belongs to bats that died while roosting locally in the karst system. Nevertheless, future taphonomic analyses will help to verify this hypothesis. The rhinolophids are represented by three species, vespertilionids by two. Most interesting is the presence of an extinct bent-winged bat, *Miniopterus* cf. *horaceki*, also known in the Early Pleistocene site of Almenara-Casablanca 1 (referred to as *Miniopterus* sp. in Sevilla and Furió, 2010). This species apparently went extinct sometime during the Early Pleistocene, probably due to the climatic changes, and is no longer part of the bat assemblages found is slightly younger sites such as the nearby Cueva Victoria (Sevilla, 2012).

Family Rhinolophidae Gray, 1825

Rhinolophids, known as Horse-shoe bats, are represented in Quibas-Sima by three species, all of them common components of Iberian Quaternary fossil bat associations since the Early Pleistocene and even earlier (Sevilla, 1991), and usually represented in low numbers. These bats most commonly roost in caves and rock crevices either as solitary individuals or building colonies.

Rhinolophus ferrumequinum (Schreber, 1774)

The Greater Horseshoe bat is the largest rhinolophid species in Europe. Its remains are easily identified for their large size and the characteristic morphology of its teeth, with robust upper canines and nyctalodont lower molars (Fig. 5G). *Rhinolophus ferrumequinum* seems to have a rather continuous presence in Quibas-Sima, although no remains of this species were recovered at unit QS-4. At QS-1.2 five teeth belonging to this species were found; at the remaining levels it is represented either by two remains (two molars in QS-2) or a single remain (QS-1.1, QS-3).

Rhinolophus euryale (Blasius, 1853)

A few teeth of the Mediterranean Horseshoe bat were recovered at two units, QS-1.2 (six teeth) and QS-4 (a single canine) (Fig. 5H–J). This species is also easily identified in fossil assemblages thanks to its typical rhinolophid morphology and smaller size. *Rhinolophus euryale* is found roosting mainly in caves surrounded by forest and shrubland. Its current geographical distribution shows a distinct affinity to warm Mediterranean conditions, and is relatively common in Quaternary Iberian sites (Sevilla, 1988).

Rhinolophus hipposideros (Bechstein, 1800)

446 The Lesser Horseshoe bat is the smallest rhinolophid species in the Palearctic. Its remains
447 are unmistakable due to their rhinolophid morphology and small size. The fragility of
448 these fossils is probably responsible for the few remains recovered in Quaternary sites,
449 although this extant species has a record that extends to the Pliocene. This species is
450 known from some Iberian sites such as Almenara-Casablanca 1 (Sevilla and Furió, 2010).
451 In Quibas-Sima a single remain was retrieved from QS-1.2 (Fig. 5K).

452 Family Vespertilionidae Gray, 1821

453 Subfamily Vespertilioninae Gray, 1821

454 *Myotis myotis* (Borkhausen, 1797)

455 The Greater Mouse-eared bat is certainly the most common bat species in the Quaternary
456 record of the Iberian Peninsula; it is present in almost all sites with fossil bats and is
457 usually represented by relatively abundant remains (Sevilla, 1988; Sevilla and López-
458 García, 2010). With a good record since the Late Pliocene, the remains of this species are
459 easy to recognise thanks to its large size, robust appearance and myotodoncy.
460 Nevertheless, it slightly overlaps in size with *Myotis blythii*, its sibling species, making
461 difficult in some cases to determine which of these two species is present in an
462 assemblage. A single canine assigned to *Myotis myotis* was found in the sediments of QS-
463 3, and a M2 in QS-4 (Fig. 5E, F). The low representation of this species in Quibas-Sima
464 could be explained by the characteristics of the cavity in which the fillings were deposited,
465 since this species is very gregarious, particularly for breeding purposes. It usually prefers
466 to roost in the ceiling of ample and relatively warm cavities, where it can be found
467 together with other species such as rhinolophids, vespertilionids and miniopterids (Dietz
468 et al., 2009). However, a predatorial origin of these remains cannot be discarded since the

469 molar from QS-4 shows clear signs of corrosion. A taphonomic analysis will be
470 performed in order to clarify if this corrosion is due to digestion or of edaphic origin.

471 *Myotis nattereri* (Kuhl, 1817)

472 Natterer's bat is also common in Pleistocene associations, although never represented in
473 large numbers and usually found together with the Greater Mouse-eared bat. Fossils of
474 this species are found already in earliest Pleistocene Iberian sites such as Almenara-
475 Casablanca 1 (Sevilla and Furió, 2010). Its remains resemble those of *Myotis myotis*, but
476 of smaller size (Fig. 5L). It can be distinguished from other medium-sized *Myotis* species
477 less common in Pleistocene cave assemblages such as *Myotis bechsteinii* for its relatively
478 smaller size, or for its more massive teeth than those of *Myotis emarginatus* or *Myotis*
479 *capaccinii*. This species has been found in the lower units of Quibas-Sima, with four
480 molars retrieved at QS-1.2, a single molar from QS-1.1 and QS-2 each, and a broken
481 mandible carrying m3 from QS-3 .

482 Family Miniopteridae Dobson, 1875

483 *Miniopterus* cf. *horaceki* Gunnel, Eiting and Geraads, 2011

484 The genus *Miniopterus* is represented at Quibas-Sima by a few remains. Practically all
485 the records belonging to this genus in Quaternary sites are assigned to extant *Miniopterus*
486 *schreibersii*, which although its current status is assessed as decreasing, it was apparently
487 common during the Pleistocene considering the number of available records for this
488 epoch in the Iberian Peninsula. A second bent-winged bat was found to be coexisting with
489 *M. schreibersii* in the Early Pleistocene site of Almenara-Casablanca 1 (Sevilla and Furió,
490 2010), with a strong morphological closeness to *M. schreibersii* but distinctly larger.
491 These features coincide with *Miniopterus horaceki* described in the Late Pliocene site of

492 Ahl al Oughlam in Morocco (Gunnell et al., 2011). The material assigned to *Miniopterus*
493 at Quibas-Sima apparently displays a larger size than that of the extant species, thus
494 suggesting it belongs to the fossil species described in Morocco (see Fig. 5A–D).
495 However, the number of remains is so far too low (a molar found at QS-1.1 and eight
496 other teeth from QS-1.2) to assign without doubt the Quibas-Sima material to *M.*
497 *horaceki*. New material obtained in future excavations will help to clarify the taxonomical
498 status of this bent-winged bat from Quibas-Sima.

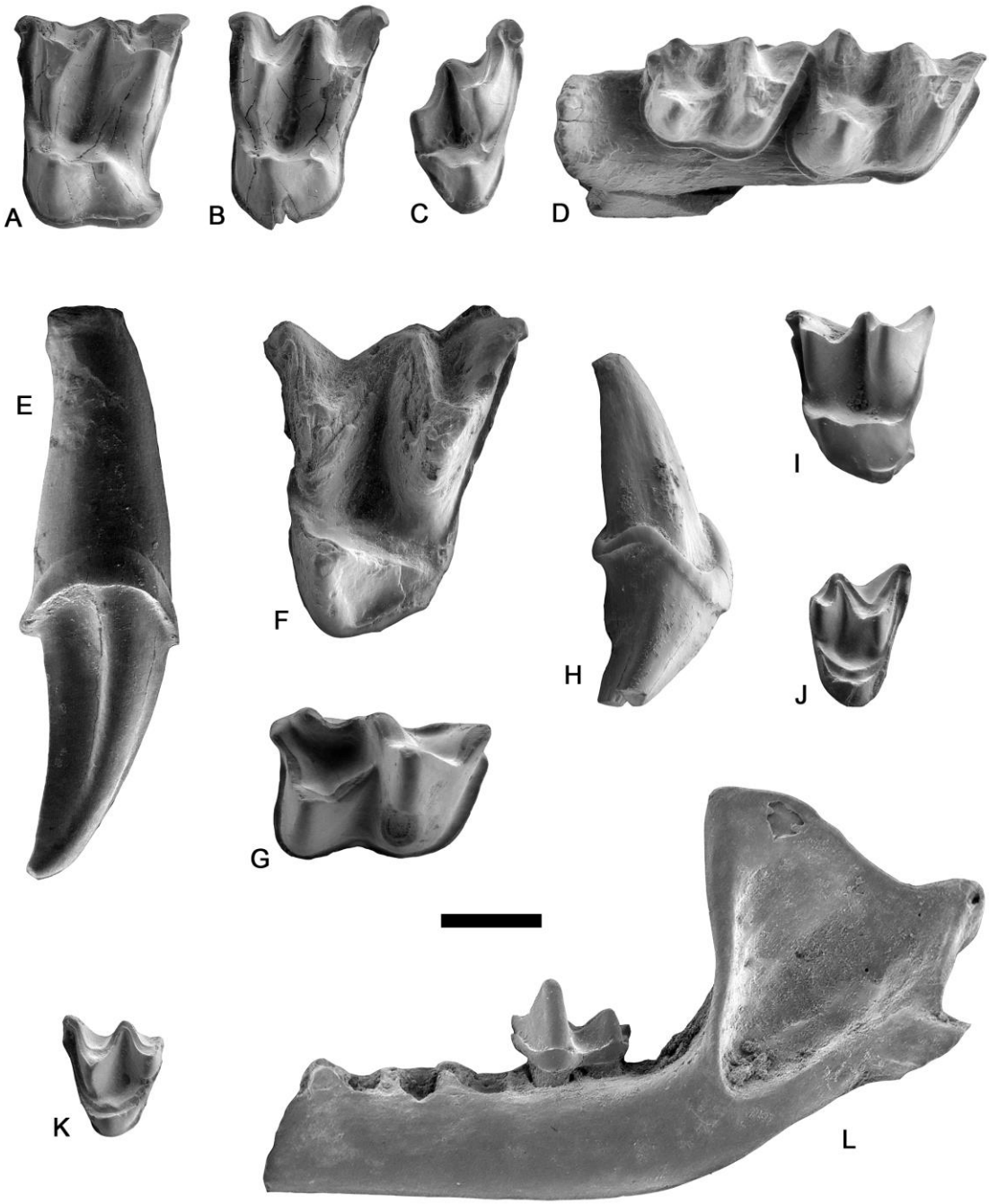

499

500 **Figure 5**. ESEM images of chiropterans from Quibas-Sima. (A-D) *Miniopterus* cf.
501 *horaceki*: A- left M1 from QS-1.2, IPHES-QS1A-Q/W2; B- left M2 from QS-1.2, IPHES-
502 QS1A-Q/W3; C- right M3 from QS-1.2, IPHES-QS1A-Q/W5; D- right mandible with
503 m2 and m3 from QS-1.2, IPHES-QS1A-Q/W7. (E-F) *Myotis myotis*: E- left upper canine
504 from QS-3 in lingual view, IPHES-QS3-Q/V16; F- left M2 from QS-4, IPHES-QS4-
505 Q/Z1. (G) *Rhinolophus ferrumequinum*: right m1 from QS-3, IPHES-QS3-Q/V15. (H-J)

Rhinolophus euryale: H- right upper canine from QS-1.2 in labial view, IPHES-QS1A-Q/W16; I- left M2 from QS-1.2, IPHES-QS1A-Q/W14; J- right M3 from QS-1.2, IPHES-QS1A-Q/W18. (K) *Rhinolophus hipposideros*: left M3 from QS-1.2, IPHES-QS1A-Q/W19. (L) *Myotis nattereri*: distal fragment of left hemimandible with m3 from QS-3, IPHES-QS3-Q/Z2. Scale bar equals 1 mm. [planned for 2 columns]

Order RODENTIA Linnaeus, 1778

Family Arvicolidae Gray, 1811

Genus *Manchenomys* Agustí, Piñero, Lozano-Fernández and Jiménez-Arenas, in press

Manchenomys orcensis Agustí, Piñero, Lozano-Fernández and Jiménez-Arenas, in press

The arvicolid representation of the whole Quibas-Sima section is restricted to the recently described rootless microtine *Manchenomys orcensis* (see Fig. 6S–V). Almost all levels have provided remains of this species. It is identified in QS-1.1 (with one molar), QS-1.2 (with 26 molars), QS-1.3 (35 molars), QS-2 (two molars), QS-3 (14 molars) and QS-4 (three molars) (dimensions are shown in Table S3). It is charaterized by the retention of a number of archaic features which enables to distinguish it from other more or less coeval microtine species. *Manchenomys orcensis* from Quibas-Sima is characterized by a very simple dental pattern, with three closed angles (T1–T3), and a simple ACC. The amount of cement in the re-entrant angles is always abundant. The AC2 is round and its leading edge does not have any enamel. The neck of AC2 is relatively wide. The lingual edge in LSA3, and particularly in LSA4, is round and slightly angular. T4 and T5 are in an alternate position but they are widely confluent. The enamel differentiation of the triangles is *Mimomys*-like: the enamel is wider on the posterior face than on the anterior side. In M3 the AL is followed by three triangles (T2, T3 and T4). T2 is narrowly

connected to AL and T3.The T4 is small and widely connected to PC. The LSA4 is absent while the BRA3 is shallow.

Manchenomys orcensis from Quibas-Sima resembles the more archaic species of *Allophaiomys* (*Allophaiomys deucalion, Allophaiomys pliocaenicus, Allophaiomys ruffoi)*, which is confirmed by the relatively short length of ACC. Besides, the morphology of the M3 is clearly of *Mimomys*-type, and different from that of *Allophaiomys chalinei* from Cueva Victoria. This latter species presents a more derived morphology than that of *Manchenomys orcensis*, particularly in the more complex M3. The first record of *Allophaiomys chalinei* is reported at the level D5 of Cal Guardiola (northern Spain) and at Cueva Victoria, both sites chronologically constrained between Jaramillo geomagnetic subchron and the Brunhes-Matuyama boundary (Minwer-Barakat et al., 2011; Gibert et al., 2016).

Manchenomys orcensis from Quibas-Sima is similar to the population of this species from Fuente Nueva 3, in the Guadix-Baza Basin (Agustí et al., in press). Moreover, the morphology of m1 of *Manchenomys orcensis* recalls that of *Manchenomys oswaldoreigi* (Agustí et al., 1993). The first occurrence of *Manchenomys oswaldoreigi* is recorded at the post-Olduvai site of Barranco de los Conejos (Guadix-Baza Basin; Agustí et al., 2013, in press). This species is also present at other coeval levels of the *Manchenomys oswaldoreigi* biozone in the Guadix-Baza Basin such as Cortes de Baza 1 and Fuentecica 5 (Agustí et al., 1999, 2015b; Oms et al., 2000a). In the nearby Granada Basin, a form close to *Manchenomys oswaldoreigi* has been recognized at the Early Pleistocene levels of Huétor Tájar 1, Huétor Tájar 8 and Tojaire 1 (García-Alix et al., 2009a, 2009b; Agustí et al., in press). The persistence of *Manchenomys orcensis* in the late Early Pleistocene can therefore be explained by a local evolution from *Manchenomys oswaldoreigi*.

Family Muridae Illiger, 1811

Apodemus sylvaticus (Linnaeus, 1758)

Apodemus sylvaticus has been reported from all levels of Quibas-Sima with microvertebrate remains, being the most abundant taxon (Fig. 6A–G). The sample from QS-1.1 consists of 13 molars, QS-1.2 of 223, QS-1.3 of 364, QS-2 of 16, QS-3 of 35, QS-4 of 10 and QS-7 of 3 molars (see measurements in Table S4). The samples show no significant changes in morphology or size along the series. They have been compared with 50 non-fossil individuals of *Apodemus sylvaticus* coming from several localities of the Iberian Peninsula kept in the National Museum of Natural History (Madrid, Spain). The teeth from Quibas-Sima and those of recent individuals of *Apodemus sylvaticus* are very similar in both size and morphology, so that the dental pattern of this species remains fairly stable over time. The only remarkable difference lies in the morphology of the t12 in the M1. In the case of the M1s from the Quibas-Sima sequence, there are two different morphotypes with variable prevalence. So that molars can develop the morphotype 1 (fig. 5B in Piñero et al., 2015) or the morphotype 2 (fig. 5C in Piñero et al., 2015). The morphotype 1 consist of the presence of a t12 laterally compressed, forming a curved lamellar structure toward the t9, presenting a t12 connected directly both with the t8 and the t9 (Fig. 6B). The morphotype 2 consist of the presence of a t12-t8 connection and a t8-t9 connection, excluding the t12-t9 union (Fig. 6C). In the latter case, some worn specimens can have the t12 joined to the t9 forming a funnel between the anterior t8-t9 connection and the posterior t12-t9. The percentage of each morphotype in the M1s from Quibas-Sima is shown in Table 3. Differently, all observed recent individuals of *Apodemus sylvaticus* uniformly show the morphotype 1.

576 Martín Suárez and Mein (1998) considered that *Apodemus sylvaticus* is a descendent of
577 *Apodemus atavus*. The latter species has a well-developed t12 and presents the
578 morphotype 2 in all the M1s. It has been directly verified when reviewing the material of
579 *Apodemus atavus* from Monte la Mesa in north-eastern Italy (early Biharian), stored at
580 the *Università degli Studi di Ferrara* (Italy). So far, it is the most abundant collection of
581 this species in Europe (Marchetti et al., 2000; Sala and Masini, 2007). We consider that
582 the high prevalence of the morphotype 2 in fossil material of *Apodemus sylvaticus* is
583 distinctive of archaic populations since it seems to be a remnant feature inherited from its
584 probable ancestor. Other archaic populations of *Apodemus sylvaticus* such as those from
585 Torrent de Vallparadís (Minwer-Barakat et al., 2011, fig. 8) and Loma Quemada-1
586 (Anchelergues Tarraco et al., 2015, fig. 1) preserve the characteristic morphotype of
587 *Apodemus atavus* in some molars. It is congruent with the relation ancestor-descendant
588 between these two species.

589 *Castillomys rivas* Martín Suárez and Mein, 1991

590 The species *Castillomys rivas* is recorded at the levels QS-1.1 (with two molars), QS-1.2
591 (41 molars), QS-1.3 (77 molars), QS-2 (three molars), QS-3 (six molars) and QS-4 (one
592 molar) (Fig. 6H–J) (measurements are shown in Table S5). All the specimens have well-
593 developed longitudinal crests, completing the connection among the tubercles of the
594 crown. The M1 generally develop t1bis and t2bis. The lower molars have a broad labial
595 cingulum separated from the protoconid by a valley. The studied teeth agree in size and
596 morphology with *Castillomys rivas* from its type locality (Loma Quemada-1; Martín
597 Suárez and Mein, 1991). Martín Suárez and Mein (1991) proposed the following
598 anagenetic evolutionary lineage: *Castillomys gracilis* – *Castillomys crusafonti* –
599 *Castillomys rivas*, being the first occurrence of *Castillomys gracilis* restricted to the early

Pliocene (Piñero and Agustí, 2019). *Castillomys rivas* has been reported along the Early Pleistocene in a number of Spanish and southern French localities. Thereby, the first populations of *Castillomys rivas* are recorded in earliest Pleistocene levels such as Tollo de Chiclana 10 and 10B (MN17, Minwer-Barakat et al., 2005) and Valdeganga 7 (MN17, Mein et al., 1978), whereas its last occurrence is recorded in the late Early Pleistocene level of Cúllar-Baza B (Agustí et al., 1999).

Family Sciuridae Fischer, 1817

Genus *Hylopetes* Thomas, 1908

Hylopetes sp.

At the Quibas-Sima succession, sciurids are represented by a relatively poor sample belonging to a single species, identified here as *Hylopetes* sp. (see Fig. 6W, X). Remains of this taxon are present in the units QS-1.2 (with two teeth), QS-1.3 (two teeth) and QS-2 (one tooth), and are absent in the remaining layers. It is a medium-sized squirrel (see dimensions in Table S6) with a relatively simple dental pattern and with the enamel of the bottom of the valleys smooth or finely pitted. This last character (clearly recognizable in the most abundant sample of the same taxon from Quibas-Cueva, which will be described in a forthcoming paper) relates the Quibas material to the Early Pleistocene species of *Hylopetes* (Reumer and van der Hoek Ostende, 2003). Other Early Pleistocene squirrels with a similar dental design, such as those of the genus *Sciurus* (*S. vulgaris*, *S. whitei*, *S. warthae*), lack this specific type of ornamentation (Hinton, 1914; Sulimski, 1964; Cuenca-Bescós, 1988).

Two species of the genus *Hylopetes* have been described from the European Early Pleistocene: *H. magistri* van der Hoek Ostende and Reumer, 2011 (described initially as

H. debruijni Reumer and van der Hoek Ostende, 2003, preoccupied by *H. debruijni* Mein & Ginsburg, 2002) and *H. marinae* Guillén Castejón, 2010. The slight differences in size and morphology between them make it impossible to confirm the specific identification of the scarce Quibas-Sima material.

It is worth mentioning that some authors consider that some species initially attributed to the genus *Hylopetes* could belong instead to *Sciurus*. This is the case of *H. magistri*, which for Colombero et al. (2014) is a representative of *Sciurus*. To justify this change in generic assignment, these authors mainly rely on the observation by Thorington et al. (2005) that enamel ornamentation is present in flying squirrels (such as those of the genus *Hylopetes*) but also in ground and tree squirrels. Following this argument, the Quibas-Sima material was initially identified as *Sciurus* aff. *magistri* (Piñero et al., 2020). However, when present in these latter squirrels, this ornamentation is less regular and different in appearance from that seen in *Hylopetes* species. For this reason, and to highlight the similarity of the Quibas-Sima material with the species originally included in *Hylopetes*, the material studied has been identified as *Hylopetes* sp.

In any case, the Quibas-Sima material is insufficient to shed light on this discussion. The description of the most abundant material from Quibas-Cueva (in a forthcoming paper) can provide relevant data to resolve this systematic uncertainty.

During the Pleistocene, the genus *Hylopetes* had a limited fossil record in the Iberian Peninsula. It was recognized in two northeastern Iberian sites: Canal Negre 1 (where two species were identified: *H. magistri* and *H. marinae*; Pliocene-Early Pleistocene, Guillén Castejón, 2010) and Canal Negre 7 (identified as *H. marinae*; Middle Pleistocene, Guillén Castejón, 2015). Taking into account the difficulties in identifying fossil squirrels and the fact that this group of rodents is usually represented by very scarce material at the sites

where it is present, some sciurid remains identified as belonging to different taxa at many other Iberian and western European sites could also be related to *Hylopetes*. However, it is out of the scope of this work to review these occurrences.

Family Gliridae Thomas, 1897

Eliomys quercinus (Linnaeus, 1766)

The family Gliridae is just represented at Quibas-Sima by *Eliomys quercinus* (see Fig. 6K–R). However, this species is present all along the sequence: QS-1.1 (two molars), QS-1.2 (37 molars and premolars), QS-1.3 (87 molars and premolars), QS-2 (four molars and premolars), QS-3 (one molar), QS-4 (one molar) and QS-7 (one molar) (measurements are shown in Table S7). This taxon is particularly abundant in the lower units, where it reaches the 14% of small mammal teeth at QS-1.3. The morphology of the teeth is very simple, the majority of lower molars already laking a posterotropid. Only one lower molar at QS-1.3 and another one at QS-1.2 display a posterotropid. Surprisingly, the only lower molar from the youngest level, QS-7, again presents a posteropropid. The absence of a posterotropid has been used to distiguish the living species *Eliomys quercinus* from the Pliocene and Early Pleistocene species *Eliomys intermedius*, which still retains a posterotropid in most of the lower molars. In southern Spain, the localities of Venta Micena 2 and Barranco León 2-3 (Guadix-Baza Basin), still present *Eliomys intermedius* (Agustí et al., 1987a; 1987b). In contrast, at the younger site of Cueva Victoria, the *Eliomys* representatives can be assigned to *Eliomys quercinus*, already lacking any evidence of posterotropid (Agustí, 1982). Therefore, the sample from the Quibas-Sima section can also be assigned to *Eliomys quercinus*. However, the scarce presence of some lower molars still retaining a posterotropid could indicate an intermediate position of the populations of Quibas-Sima between those of the Early Pleistocene sites of Guadix-Baza

(Venta Micena 2, Barranco León 2-3) and the one of Cueva Victoria. *Eliomys quercinus* underwent a great expansion throughout Europe during the entire Pleistocene.

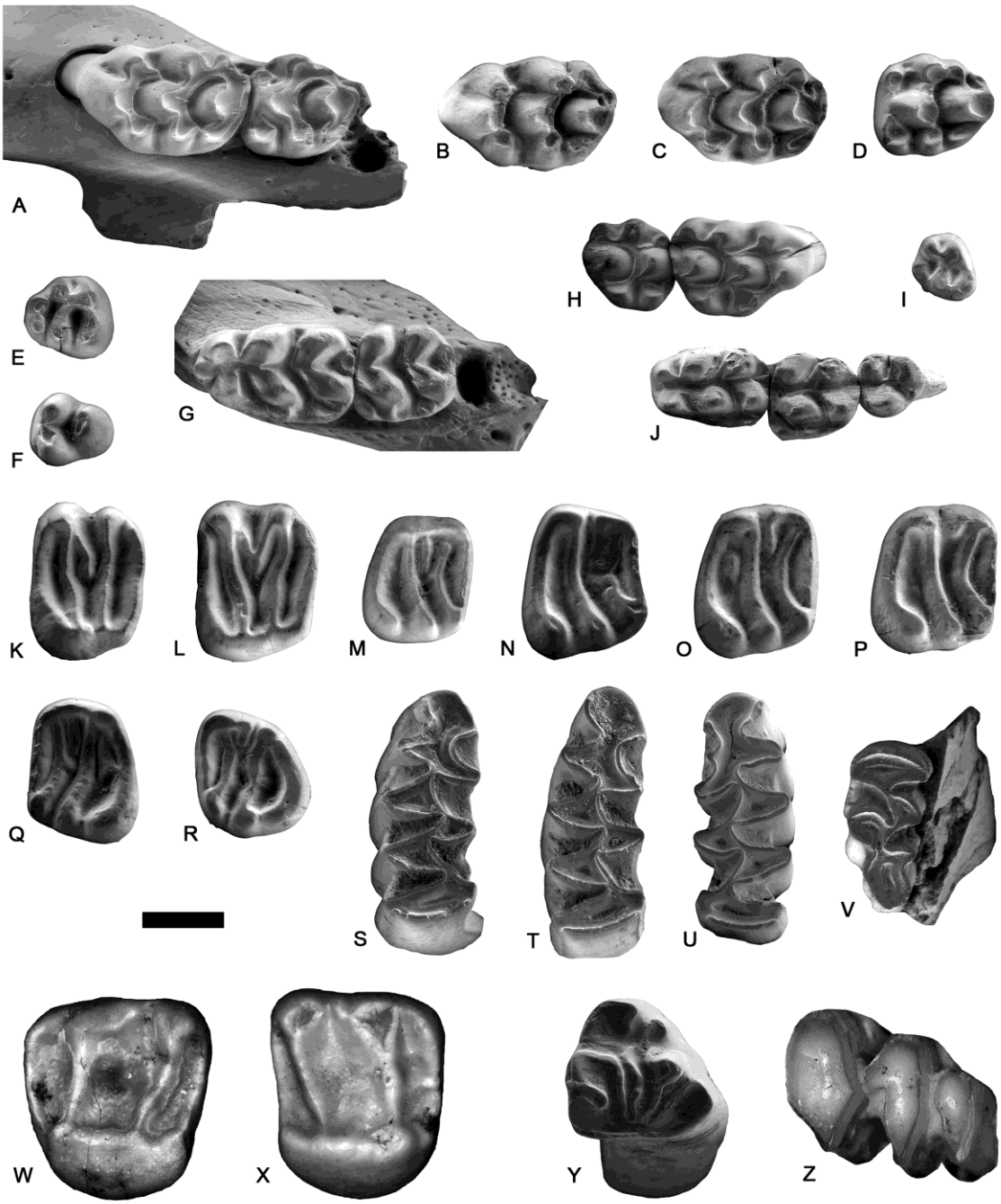

Figure 6. ESEM photographs of rodents and lagomorphs from Quibas-Sima. (A-G) *Apodemus sylvaticus*: A- left maxilla with M1 and M2 from QS-3, IPHES-QS3-R/P25; B- left M1 from QS-1.3, IPHES-QS1Z-R/H13; C- left M1 from QS-1.3, IPHES-QS1Z-R/H2; D, left M2 from QS-1.3, IPHES-QS1Z-R/H83; E- right M3 from QS-1.3, IPHES-

678 QS1Z-R/H142; F- left m3 from QS-1.3, IPHES-QS1Z-R/I165; G- left mandible with m1
679 and m2 from QS-1.3, IPHES-QS1Z-R/I1. (H-J) *Castillomys rivas*: H- right M1 and M2
680 from QS-1.3, IPHES-QS1Z-R/J1; I- right M3 from QS-1.3, IPHES-QS1Z-R/J13; J- left
681 m1, m2 and m3 from QS-1.3, IPHES-QS1Z-R/J31. (K-R) *Eliomys quercinus*: K- left M1-
682 2 from QS-1.2, IPHES-QS1A-R/G6; L- left M1-2 from QS-1.3, IPHES-QS1Z-R/L19; M-
683 right m1-2 from QS-1.3, IPHES-QS1Z-R/M57; N- right m1-2 from QS-1.2, IPHES-
684 QS1A-R/G26; O- right m1-2 from QS-1.3, IPHES-QS1Z-R/L51; P- right m1-2 from QS-
685 1.3, IPHES-QS1Z-R/M61; Q- left m1-2 from QS-7, IPHES-QS7-R/T4; R- left m3 from
686 QS-1.3, IPHES-QS1Z-R/M82. (S-V) *Manchenomys orcensis*: S- right m1 from QS-3,
687 IPHES-QS3-R/Q7; T- right m1, IPHES-QS3-R/Q6; U- left m1 from QS-3, IPHES-QS3-
688 R/Q1; V- left M3 from QS-1.3, IPHES-QS1Z-R/K32. (W-X) *Hylopetes* sp.: W- left P4
689 from QS-1.2 (IPHES-QS1A-R/AB1); X- right M1-2 from QS-1.2, IPHES-QS1A-R/AB2.
690 (Y) *Oryctolagus* cf. *giberti*: left upper molariform from QS-3, IPHES-QS3-L/V8. (Z)
691 *Prolagus calpensis*: right p3 and p4 from QS-3, IPHES-QS3-L/V12. Scale bar equals 1
692 mm. [planned for 2 columns]

693 Order LAGOMORPHA Brandt, 1855

694 Family Leporidae Fischer, 1817

695 *Oryctolagus* cf. *giberti* De Marfà, 2008

696 Remains of *Oryctolagus* cf. *giberti* are present throughout all the recognized stratigraphic
697 units with faunal content, excepting QS-1.1 and QS-7. The sample from QS-1.2 is
698 composed by six teeth, QS-1.3 by 11 teeth, QS-2 by five teeth, QS-3 by 15 teeth, and QS-
699 4 by 12 teeth (Fig. 6Y) (see dimensions in Table S8). The specimens share with the
700 sample from Cueva Victoria (the type locality of the species) the size and morphology of
701 the teeth, which are very similar to the recent *Oryctolagus cuniculus* (see De Marfà,

2008). At the p3, the anteroconids are nearly symmetrical, a trait typical of *Oryctolagus* that distinguish it from *Lepus*. All the upper molariforms show deep hypoflexids which extend beyond the midpoints of the width of the teeth, and having crenelated anterior margins. In *Oryctolagus laynensis*, the oldest known *Oryctolagus* species (early Pliocene), the hypoflexid is shallower and never reach the half of the width of the teeth. Teeth from the Quibas-Sima are smaller than those of *Oryctolagus lacosti*, *O. valdarnensis* and *Oryctolagus burgi*.

De Marfà (2008) suggested that some Early Pleistocene Iberian rabbit samples previously identified as belonging to different species, such as *Oryctolagus* cf. *laynensis* (Córdoba and Islas Medas sites) and *Oryctolagus* cf. *lacosti* (Bagur) (López-Martínez, 1989), could be related to *Oryctolagus giberti*. If this proposal is confirmed, only a single species of rabbit, *Oryctolagus giberti*, would be present in the Iberian Peninsula during the Early Pleistocene. Differences between *Oryctolagus giberti* and *Oryctolagus cuniculus* are found mainly in the postcranial skeleton, while the dentition is nearly identical in both species. The postcranial remains of the Quibas-Sima section are not yet available for study. For this reason, we tentatively identify the rabbit remains as *Oryctolagus* cf. *giberti* until the postcranial skeleton can be studied.

Oryctolagus giberti has been recorded in a number of Early Pleistocene French and Spanish localities: Cueva Victoria (De Marfà, 2008), Sima del Elefante Lower Red Unit (Cuenca-Bescós et al., 2010), Bois de Riquet (Pelletier et al., 2015) and Cueva Negra del Estrecho del Río Quípar (López-Jiménez et al., 2020). All these localities are chronologically placed around the Jaramillo subchron (late Early Pleistocene). However, if the proposal of De Marfà (2008) is correct and this species is also present in sites such as Córdoba and Islas Medas (MN17), the record of *Oryctolagus giberti* would extend

throughout much of the Early Pleistocene. According to De Marfà (2008), *Oryctolagus giberti* is an intermediate species in the anagenetic lineage that begins with *Oryctolagus laynensis* and ends with *Oryctolagus cuniculus*. Therefore, *Oryctolagus giberti* is a species closely related to the European rabbit.

Family Ochotonidae Thomas, 1896

Prolagus calpensis Major, 1905

There are *Prolagus* remains in QS-1.2 (six molars and premolars), QS-1.3 (three teeth), QS-3 (one mandible with the complete toothrow and other three isolated teeth), and QS-4 (one molar) (Fig. 6Z) (see measurements in Table S9). They are slightly less abundant than those of *Oryctolagus* and include three p3s, the main diagnostic element. They show large and ellipsoidal anteroconids in which labial inflections can be shallow or absent. The crochet is absent. Both the size and morphology agree with the species *Prolagus calpensis*, the most frequent *Prolagus* species in the Iberian Peninsula during the Pleistocene. At the Quibas-Sima section, remains of *Prolagus calpensis* are present throughout most of the recognized stratigraphic units. *Prolagus calpensis* is a common species in sites from the Iberian Peninsula over a long time-span ranging from the Late Pliocene (Moreda, MN16) until the Middle Pleistocene (El Carmel) (López-Martínez, 1989).

5. Biostratigraphic correlations with other Spanish localities

The high evolutionary rates and rapid diversification of small mammals during the Quaternary, and particularly arvicolids, make them an excellent tool for correlating European Pleistocene faunas (e.g. Minwer-Barakat et al., 2011, Agustí et al., 2015b). Morphological evolutionary changes among species of small mammals are frequently

749 reflected in the molars, so they can be traced in the fossil record. Thereby, the relative
750 age of units QS-1 to QS-4 can be indirectly estimated based on their small mammal
751 content (and assuming that sediment and fossil deposition are coeval for these units). As
752 for QS-7, with the only presence of two living species (*Apodemus sylvaticus* and *Eliomys*
753 *quercinus*), likely due to taphonomic bias, other methods for determining the age have
754 been used (Piñero et al., 2020). There is no evidence as far as taxonomic composition or
755 morphometric features of teeth (see Tables S4, S7) suggesting that the uppermost QS-7
756 unit biostratigraphically differs from the lowest units. Instead, the whole small mammal
757 succession from QS-1 to QS-7 is very homogeneous, indicating that it belongs to a single
758 biozone. In this section, we make an extensive biostratigraphic correlation of the four
759 lowest units of Quibas-Sima with several Early Pleistocene Iberian Peninsula localities
760 based on the occurrence of diverse rodent and shrew species.

761 The composition of the small mammal assemblage from QS-1 to QS-4 remains overall
762 unchanged along the sequence, suggesting a limited time span from bottom to top. The
763 most relevant taxon with biostratigraphic value present at Quibas-Sima is *Manchenomys*
764 *orcensis*. The first occurrence of the genus *Manchenomys* is recorded at the post-Olduvai
765 locality of Barranco de los Conejos (Guadix-Baza Basin; Agustí et al., 2013), with the
766 species *Manchenomys oswaldoreigi*, ancestor of *Manchenomys orcensis* (Agustí et al., in
767 press). This suggests that Quibas-Sima is located in a higher stratigraphic position than
768 Barranco de los Conejos, being therefore younger than the Olduvai subchron (1.94–1.78
769 Ma; Channell et al., 2020). In the Guadix-Baza Basin, *Manchenomys oswaldoreigi* is also
770 present at the levels of Cortes de Baza 1 and Fuentecica 5 (*Manchenomys oswaldoreigi*
771 biozone, between roughly 1.8 and 1.6 Ma; Agustí et al., 1999, 2015b, in press; Oms et
772 al., 2000a), again indicating an older age than Quibas-Sima (see Fig. 7). *Manchenomys*
773 *oswaldoreigi* is absent at the sites of Venta Micena, Fuente Nueva 2 and Orce 7, all

774 correlated with the *Allophaiomys ruffoi* biozone from the Guadix-Baza Basin (Agustí et
775 al., 2010, 2015b). However, evidence suggests that some populations close to
776 *Manchenomys oswaldoreigi* remained during the time span represented by the
777 *Allophaiomys ruffoi* biozone, between ca. 1.6 and 1.4 Ma (Agustí et al., 2015b, in press).
778 Again, these sites are biostratigraphically older than Quibas-Sima.

779 The first occurrence of *Manchenomys orcensis* is recorded at the late Early Pleistocene
780 localities of Fuente Nueva 3 and Barranco León, where the earliest hominin presence in
781 western Europe has been reported. These sites are dated to 1.4–1.2 Ma (Oms et al., 2011;
782 Duval et al., 2012a; Toro-Moyano et al., 2013; Lozano-Fernández et al., 2015). The lower
783 part of the Quibas-Sima section shares with Fuente Nueva 3 and Barranco Leon the
784 presence of *Manchenomys orcensis* (among others), which suggests a roughly similar age.
785 However, in Fuente Nueva 3, the shrew *Asoriculus* has not yet been replaced by *Neomys*,
786 indicating that the base of Quibas-Sima is not older than ca. 1.2 Ma. The occurrence of
787 *Asoriculus* in Sima del Elefante TE7–TE14 (Atapuerca karstic complex) also suggests a
788 slightly older age than the lowermost unit of Quibas-Sima (Rofes and Cuenca-Bescós,
789 2006; Cuenca-Bescós et al., 2015).

790 A further element with biostratigraphic value found at Quibas-Sima is *Castillomys rivas*.
791 The last presence of this murid is reported at the level Cúllar-Baza B (Agustí et al., 1999),
792 placed in the uppermost Matuyama chron, shortly before the Matuyama-Bruhnes
793 boundary (0.99–0.78 Ma; Channell et al., 2020). At the Atapuerca karstic complex
794 (Cuenca-Bescós et al., 2015), *Castillomys* is present in Sima del Elefante (TE7–TE14),
795 but absent in the younger lower layers of Gran Dolina (TD4 to TD7). This indicates that
796 the base of Quibas-Sima is located in a somewhat lower stratigraphic position than TD4.
797 TD4–TD7 post-date the Jaramillo subchron but pre-date the Matuyama-Bruhnes

798 boundary (Parés and Pérez-González, 1999; Parés et al., 2018), while a recent study
799 indicates that these sedimentary units most likely rapidly deposited in <100 ka, about 0.8-
800 0.9 Ma ago (Duval et al., submitted). The nearby sites of Cueva Victoria and Cueva Negra
801 have also been correlated with the uppermost Matuyama chron, to about 0.9 Ma (Gibert
802 et al., 2016; Walker et al., 2020). In these sites, the more advanced arvicolid *Allophaiomys*
803 *chalinei* is already present, pointing to a younger age than the Quibas-Sima. This is also
804 supported by the absence of *Castillomys rivas* in Cueva Negra, despite this locality has
805 yielded a huge amount of small mammal teeth (López-Jiménez et al., 2020).

806 The levels EVT12 and EVT10 from the section of Vallparadís (Minwer-Barakat et al.
807 2011) were correlated with the Jaramillo subchron (Madurell-Malapeira et al., 2010;
808 Minwer-Barakat et al. 2011). *Iberomys huescarensis* is already present at these localities,
809 an arvicolid species common in latest Early Pleistocene sites such as Huéscar 1 and Loma
810 Quemada in the Guadix-Baza Basin (Agustí et al., 2015b) and Gran Dolina (TD3/4, TD5,
811 TD6 and TD8) in Atapuerca (Cuenca-Bescós et al., 2015). However, *I. huescarensis* has
812 not been reported at Quibas-Sima, suggesting a lower stratigraphic position. The first
813 occurrence of this species probably took place between the deposition of QS-4 and
814 EVT12 (Fig. 7).

815 Therefore, based on biostratigraphic criteria, the units QS-1 to QS-4 post-date the Olduvai
816 subchron, having an intermediate stratigraphic position between the late Early Pleistocene
817 sites of Fuente Nueva 3 (at about 1.2 Ma) and Cueva Victoria (at roughly 0.9 Ma) (see
818 Fig. 7).

819 **6. Combined U-series/ESR dating**

820 Repeated ESR measurements returned excellent intensity precision (1.5%), resulting in a
821 variability of <5 % for the D_E values (Table 1). Fitting performed with the SSE function

822 and data weighting by $1/I^2$ yield a D_E estimate of 1835 ± 143 Gy (Fig. 2). The
823 corresponding D_{max}/D_E ratio of 1.6 falls within the recommended range (0.9-1.8) by
824 Duval and Grün (2016). Additional fitting performed with data weighting by $1/s^2$ return
825 a D_E value lower by about 6%, but within 1σ agreement with the previous dose estimate.
826 This illustrates the limited impact of fitting options on D_E results.

827 Solution U-series analyses of powdered dental tissues returned apparent ages ranging
828 from 270 to 309 ka, depending on the dental tissue considered (Table 2). These results
829 should be regarded as minimum age constraints for the fossil tooth. The limited detrital
830 Th content has virtually no impact on the calculated ages (<1 ka). Because dental tissues
831 show no evidence of uranium leaching since they both return finite U-series ages
832 estimates, the US model defined by Grün et al. (1988) can be employed for combined U-
833 series/ESR dating. However, given the relatively high uranium concentration (>5 ppm)
834 measured in the enamel, the sample does not fully meet the suitability criteria for ESR
835 dating defined by Duval et al. (2012a).

836 Age calculation return a combined US-ESR age estimate of 369 +28 -53 ka. This result
837 should be only be interpreted as a minimum age constraint given the massive internal
838 dose rate component calculated, which represents 72% of the total dose rate. This
839 overestimated value results from the high uranium concentration in the enamel, which
840 was anticipated earlier to significantly bias the age calculation: this is a well-known issue
841 in ESR dating that is most likely related with the inverse correlation of the alpha
842 efficiency with uranium concentration in the enamel, as soon as the latter exceeds 2-3
843 ppm (see Bahain et al., 1992; Duval et al., 2012a), eventually resulting in an
844 overestimation of the total dose rate and thus an underestimated age.

845 We acknowledge the existing uncertainty around the gamma dose rate evaluation in the
846 absence of *in situ* measurements. This uncertainty has currently, however, a limited

847 impact on the calculated ages given the reduced weight of the gamma component in the
848 total dose rate (< 10%).

849 Finally, one additional age calculation was performed using the CSUS model, resulting
850 in an estimate of 1431 ± 278 ka (Table 1). This model is based on the assumption that all
851 of the uranium migrated into the sample at a time given by the closed system U-series age
852 (Grün 2000b). Typically, the CSUS-ESR age is the maximum age that can be derived
853 from a given U-series and ESR data set. Consequently, the US and CSUS models
854 encompass all possible uptake scenarios, and the true age of the tooth lies somewhere
855 between ca. 370 and 1430 ka. This massive age difference (> 1Ma) illustrates the
856 significant impact of the uncertainty associated to the uranium uptake process when the
857 total dose rate is dominated by the various U sources in the dental tissues, as frequently
858 observed in Early Pleistocene samples (see also Walker et al., 2020).

859 The Quibas-Sima section recorded a succession of various intervals of different
860 geomagnetic polarities (Fig. 1), with two reversed polarity intervals at the bottom (QS-1)
861 and top of the sequence (QS-6 and QS-7), and a normal polarity interval in between (units
862 QS-2, QS-3, QS-4, QS-5). The latter was previously correlated to the Jaramillo subchron
863 (1.07–0.99 Ma) by Piñero et al. (2020). The age range given by the US-ESR and CSUS-
864 ESR age estimates (370–1430 ka) is therefore compatible with the independent
865 biostratigraphical and magnetostratigraphic evidence, but also unambiguously shows that
866 the palaeontological level is younger than the Olduvai subchron (1.94–1.78 Ma),
867 confirming previous conclusions (Fig. 7).

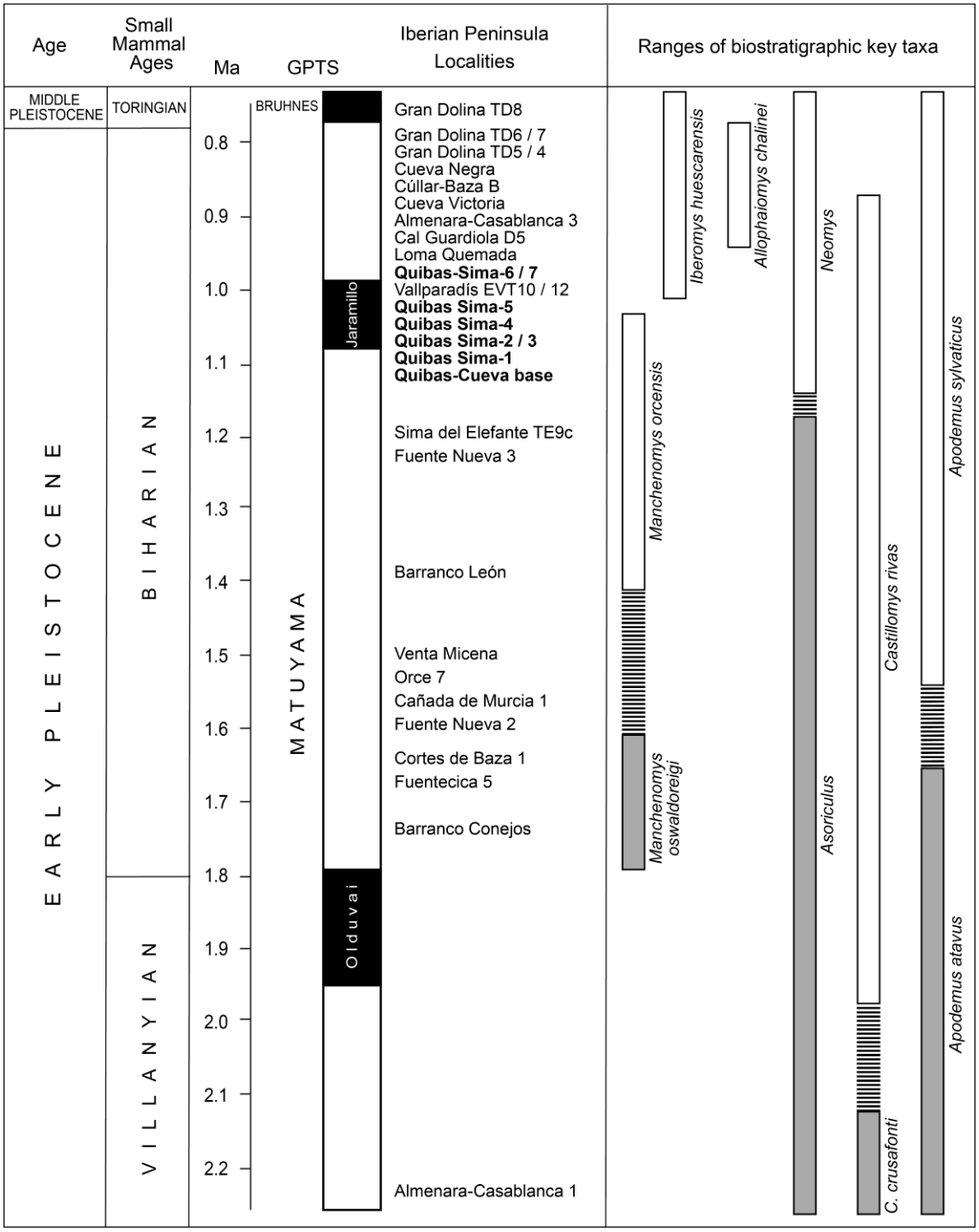

868

869 **Figure 7**. Biostratigraphic correlation of several Iberian localities and location of the
870 Quibas-Sima units (QS-1 to QS-7). All localities except for Cañada de Murcia-1,
871 Fuentecica-5, Fuente Nueva-2 and Almenara-Casablanca 3 are calibrated with
872 paleomagnetic data (Oms et al., 1994, 2000b; Agustí et al., 1999, 2011, 2013; Gibert et
873 al., 2006, 2016; Scott et al., 2007; Madurell-Malapeira et al., 2010; Minwer-Barakat et

al., 2011; Álvarez et al., 2015; Parés et al., 2018; Piñero et al., 2020). GPTS (Geomagnetic Polarity Time Scale) shows Matuyama and Bruhnes chrons, and two normal polarity intervals within Matuyama: subchrons Olduvai (1.94–1.78 Ma) and Jaramillo (1.07–0.99 Ma). [planned for 1 column]

7. Implications for the timing of the sedimentary infill

With the identification of 4.7 m-thick Jaramillo subchron (1.07–0.99 Ma; Channell et al., 2020) in the sedimentary section, a mean sedimentation rate (SR) of 5.9 cm/kyr may be calculated for the deposits positioned between the base of QS-2 and the top of QS-5 unit. The extrapolation of this value to the bottom and top of the sequence indicates that the sedimentary infill of Quibas-Sima might be chronologically constrained to between ca. 1.12 and 0.93 Ma, respectively. Interestingly, these results are very consistent with biostratigraphic correlations positioning the sequence between Fuente Nueva 3 (ca. 1.2 Ma), and Cueva Victoria, Cueva Negra, and Gran Dolina TD4–TD8 (all $\leq$0.9 Ma; Duval et al., 2012; Gibert et al., 2016; Rodríguez et al., 2011). They also imply that the sedimentary sequence was deposited in a relatively short time (ca. 190 kyr).

On the one hand, we do acknowledge that both the SR and the extrapolated numerical ages should be regarded as mostly indicative given their non-negligible associated uncertainties (see an overview in Duval et al., 2021). For example, the palaeomagnetic sampling resolution as well as the relative scatter in the VGP values along the sequence may impact the vertical position of the magnetic inversions. The main source of uncertainty is probably related to the assumption of a constant sedimentation over the whole sequence, which is most likely an oversimplified hypothesis in karstic environment. In particular, sedimentary characteristics of QS-1 unit suggest a slower sedimentation rate than that of the upper units. Furthermore, the speleothem at the top of

898 QS-1 (Fig. 1B) indicates not only some abrupt change in the sedimentation dynamics of
899 the infill, but also a chronological hiatus with the rest of the sequence above. A similar
900 interpretation can be made from the speleothem positioned at the boundary between QS-
901 4 and QS-5 (Fig. 1B).

902 On the other hand, the independent evidence based on the biostratigraphic record indicate
903 there is no difference between the pre-Jaramillo (QS-1), Jaramillo (QS-2 to QS-5) and
904 post-Jaramillo units (QS-6 and QS-7). In other word, the stratigraphic homogeneity of the
905 small mammal fossil assemblage strongly support the hypothesis of a relatively rapid
906 deposition of the whole sedimentary infill, as per suggested by the SR estimate. This
907 indirectly suggests that the variable sedimentation rate or the sedimentary hiatus
908 mentioned above are of limited magnitude/duration. Moreover, the Jaramillo subchron
909 represents about 1/3 of the thickness of the whole sedimentary infill, limiting thus the
910 magnitude (<3 m to the bottom and <4 m to the top) and the associated uncertainty of the
911 extrapolation.

912 Finally, the estimated SR value of 5.9 cm/kyr should be regarded as a minimum value, as
913 it is unlikely that the magnetic inversions observed in the local magnetostratigraphy do
914 correspond to the known geomagnetic boundaries of Jaramillo. This implies that the 4.7-
915 m thick deposits would correspond to a shorter time interval, resulting in a larger
916 sedimentation rate. Consequently, the extrapolated ages obtained for the bottom and top
917 of the sequence should be interpreted as maximum and minimum age constraints,
918 respectively (<1.12 Ma and >0.93 Ma). The resulting estimated duration for the
919 sedimentary infill would be <190 kyr.

920 To sum up, while we do acknowledge the intrinsic uncertainty associated to the estimation
921 of a sedimentation rate in karstic environment, there is nevertheless a series of evidence

suggesting that whole the sedimentary infill of Quibas-Sima most likely deposited in less than 200 kyr, between 1.1 and 0.9 Ma ago.

8. Conclusions

Quibas-Sima is one of the very few archaeo-palaeontological localities in Europe where the Jaramillo subchron has been undoubtedly identified. Based on the combination of magnetostratigraphy, biostratigraphy and numerical dating, the age of the sedimentary infill at Quibas-Sima, can be estimated to between 1.2 and 0.78 Ma. Based on an estimation of the sedimentation rate during the Jaramillo subchron, these broad chronological constraints may be confidently refined to approx. 1.1–0.9 Ma for the whole sequence. While we acknowledge the existing uncertainty associated to this age range, it is nevertheless consistent with biostratigraphic evidence indicating that all stratigraphic units most likely do not significantly differ from a chronological point of view. Both independent proxies (biostratigraphy and the sedimentation rate) strongly suggest that the sedimentary sequence covers a relatively short time interval (<200 kyr), much shorter than any other localities of the Iberian Peninsula such as Vallparadís (Minwer-Barakat et al., 2011) and Atapuerca Gran Dolina (Parés et al., 2018).

The resolution of this preliminary age-depth model can be further improved in the future by providing more chronostratigraphic tie points along the sedimentary sequence. This may be achieved by employing a multi-technique dating approach using combined U-series/ESR and U-Pb methods. While the first attempt of combined U-Series/ESR dating has yielded promising age results that are compatible with the independent age control derived from the magnetostratigraphy and biostratigraphy, we nevertheless do acknowledge that the significant associated uncertainty is not satisfactory, and must be reduced. To do so, pre-screening fossil teeth using high resolution Laser Ablation ICP-

MC U-series analyses is essential, as usually recommended for Early Pleistocene samples by Duval et al. (2012b). Several samples will be selected and analysed accordingly: those showing suitable characteristics for combined U-series/ESR dating (i.e., (i) low uranium concentration in the enamel and (ii) absence of uranium leaching in dental tissues) will eventually be dated while the others will be discarded. Moreover, additional numerical age constraints will be tentatively obtained by dating the various speleothem layers identified along the sequence (Fig. 1) using U-Pb method, following a similar approach to Parés et al. (2018). To conclude, Quibas-Sima offers a unique high-resolution small mammal record around the Jaramillo subchron time range, and probably one of the longest and most complete pre-Jaramillo to Jaramillo continental vertebrate succession in Europe. Chronologically positioned within the so-called Early-Middle Pleistocene transition (Head and Gibbard, 2015), a critical time interval as far as the Earth's climate cyclicity, and for human dispersals in western Europe (e.g., Carbonell et al., 2008; Toro-Moyano et al., 2013; Muttoni et al., 2010), Quibas-Sima has now become a reference locality to improve our knowledge on the climatic and faunal events that occurred around 1 Ma at the Iberian Peninsula.

Data availability

Measurements of the teeth of the taxa studied in this work are provided in Supplementary Tables S1-S9.

Declaration of competing interest

The authors declare that they have no known competing financial interests or personal relationships that could have appeared to influence the work reported in this paper.

Acknowledgements

This work was supported by the the Comunidad Autónoma de la Región de Murcia (ARQ115/2018, Subvención para la Investigación e Intervención en el Patrimonio Arqueológico y Paleontológico de la Región de Murcia), the Palarq Foundation, the Spanish Agencia Estatal de Investigación and the European Regional Development Fund of the European Union (AEI/FEDER EU, PID2020-117289GB-I00), the Spanish Ministry of Science and Innovation (MICINN/FEDER, CGL2016-75109-P), and Generalitat de Catalunya (AGAUR 2017/SGR/859). The Institut Català de Paleoecologia Humana i Evolució Social (IPHES-CERCA) has received financial support from the Spanish Ministry of Science and Innovation through the "María de Maeztu" program for Units of Excellence (CEX2019-000945-M). PP was beneficiary of a postdoctoral contract from the "María de Maeztu" program. The U-series and ESR dating analyses have been funded by the Spanish Ramón y Cajal Fellowship RYC2018-025221-I. We are grateful to María Jesús Alonso Escarza and Javier Iglesias Cibanal, CENIEH, technical support associated to the ESR dating analytical procedure. The solution U-series dating analyses were carried out within the framework of the existing Brisbane Geochronology Alliance between Griffith University, University of Queensland and Queensland University of Technology. We gratefully acknowledge support of this work by Gregorio Romero and the Servicio de Patrimonio Histórico de la Dirección General de Bienes Culturales de la Región de Murcia. We would like to express our thanks to the Quibas excavation team, who helped with the extraction, sieving, and washing of sediments. The authors wish to thank the Town Hall of Abanilla for their support and facilities in conducting research at the Quibas site. We thank Dr. Raef Minwer-Barakat and one anonymous reviewer for constructive comments on an earlier version of the manuscript.

References

Alba DM, Carlos-Calero, JA Mancheño MA, Montoya P, Morales J, Rook L. 2011. Fossil

994 remains of *Macaca sylvanus florentina* (Cocchi, 1872) (Primates, Cercopithecidae) from
995 the Early Pleistocene of Quibas (Murcia, Spain). *Journal Human Evolution* **61**: 703–718.

996 Agustí J. 1982. Los roedores (Mammalia) del Pleistoceno inferior de la Cueva Victoria
997 (Murcia, España). *Endins* **9**: 49–55.

998 Agustí J, Moyà Solà S, Martín-Suárez E, Marín M. 1987a. Faunas de mamíferos en el
999 Pleistoceno inferior de la región de Orce (Granada, España). *Paleontologia i Evolució,*
1000 *Memòria Especial* **1**: 73–86.

1001 Agustí J, Arbiol S, Martín-Suárez E. 1987b: Roedores y lagomorfos (Mammalia) del
1002 Pleistoceno inferior de Venta Micena (depresión de Guadix Baza, Granada).
1003 *Paleontologia i Evolució, Memòria Especial* **1**: 95–107.

1004 Agustí J, Castillo C, Galobart A. 1993. Heterochronic evolution in the Late Pliocene-
1005 Early Pleistocene arvicolids of the Mediterranean area. *Quaternary International* **19**: 51–
1006 56.

1007 Agustí J, Oms O, Parés JM. 1999. Calibration of the Early-Middle Pleistocene transition
1008 in the continental beds of the Guadix–Baza Basin (SE Spain). *Quaternary Science*
1009 *Reviews* **18**: 1409–1417.

1010 Agustí J, Blain H-A, Furió M, De Marfà R, Santos-Cubedo A. 2010. The early Pleistocene
1011 small vertebrate succession from the Orce region (Guadix-Baza Basin, SE Spain) and its
1012 bearing on the first human occupation of Europe. *Quaternary International* **223**–**224**:
1013 162–169.

1014 Agustí J, Santos-Cubedo A, Furió M, De Marfá R, Blain H-A, Oms O, Sevilla P. 2011.
1015 The late Neogene-early Quaternary small vertebrate succession from the Almenara-

1016 Casablanca karst complex (Castellón, Eastern Spain). Chronologic and paleoclimatic
1017 context. *Quaternary International* **243**: 183–191.

1018 Agustí J, Blain H-A, Furió M, De Marfá R, Martínez-Navarro B, Oms O. 2013. Early
1019 Pleistocene environments and vertebrate dispersals in Western Europe: the case of
1020 Barranco de los Conejos (Guadix-Baza Basin, SE Spain). *Quaternary International* **295**:
1021 59–68.

1022 Agustí J, Blain H-A, Lozano-Fernández I, Piñero P, Oms O, Furió M, Blanco A, López-
1023 García JM, Sala R. 2015a. Chronological and environmental context of the first hominin
1024 dispersal into Western Europe: The case of Barranco León (Guadix-Baza Basin, SE
1025 Spain). *Journal of Human Evolution* **87**: 87–94.

1026 Agustí J, Lozano-Fernández I, Oms O, Piñero P, Furió M, Blain H-A, López-García, JM,
1027 Martínez-Navarro B. 2015b. Early to Middle Pleistocene rodent biostratigraphy of the
1028 Guadix-Baza basin (SE Spain). *Quaternary International* **389**: 139–147.

1029 Agustí J, Piñero P, Lozano-Fernández I, Jiménez-Arenas JM. In press. A new genus and
1030 species of arvicolid rodent (Mammalia) from the Early Pleistocene of Spain. *Comptes*
1031 *Rendus Palevol*.

1032 Álvarez C, Parés JM, Granger D, Duval M, Sala R, Toro I. 2015. New
1033 magnetostratigraphic and numerical age of the Fuente Nueva-3 site (Guadix-Baza basin,
1034 Spain). *Quaternary International* **389**: 224–234.

1035 Angelone C, Sesé C. 2009. New characters for species discrimination within the genus
1036 *Prolagus* (Ochotonidae, Lagomorpha, Mammalia). *Journal of Paleontology* **83**: 80–88.

1037 Anchelergues Tarraco A, Martín-Suárez E, Freudenthal M. 2015. Muridae (Rodentia)
1038 from the early Pleistocene of Loma Quemada-1 (Granada, Spain). *Palaeobiodiversity and*
1039 *Palaeoenvironments* **95**: 347–352.

1040 Bahain J-J, Yokoyama Y, Falguères C, Sarcia MN. 1992. ESR dating of tooth enamel: a
1041 comparison with K–Ar dating. *Quaternary Science Reviews* **11**: 245–250.

1042 Blain H-A, Bailon S. 2019. Extirpation of *Ophisaurus* (Anguimorpha, Anguidae) in
1043 Western Europe in the context of the disappearance of subtropical ecosystems at the
1044 Early-Middle Pleistocene transition. *Palaeogeography, Palaeoclimatology,*
1045 *Palaeoecology* **520**: 96–13.

1046 Blain H-A, Bailon S, Agustí J, Piñero-García P, Lozano-Fernández I, Laplana C, Sevilla
1047 P, López-García JM, Romero G, Mancheño MA. 2014. Youngest agamid lizards from
1048 western Europe (Sierra de Quibas, Spain, late Early Pleistocene). *Acta Palaeontologica*
1049 *Polonica* **59**: 873–878.

1050 Botka D, Mészáros L. 2017. *Asoriculus* and *Neomys* (Mammalia, Soricidae) remains from
1051 the late Early Pleistocene Somssich Hill 2 locality (Villány Hills, Southern Hungary).
1052 *Fragmenta Palaeontologica Hungarica* **34**: 105–125.

1053 Carbonell E, Bermúdez de Castro JM, Parés JM, Pérez-González A, Cuenca-Bescós G,
1054 Ollé A, Mosquera M, Huguet R, Made J van der, Rosas A, Sala R, Vallverdú J, García N,
1055 Granger DE, Martinón-Torres M, Rodríguez XP, Stock GM, Vergès JM, Allué E,
1056 Burjachs F, Cáceres I, Canals A, Benito A, Díez C, Lozano M, Mateos A, Navazo M,
1057 Rodríguez J, Rosell J, Arsuaga JL. 2008. The first hominin of Europe. *Nature* **452**: 465–
1058 469.

1059 Carlos-Calero JA, Montoya P, Mancheño MA, Morales J. 2006a. Presencia de *Vulpes*

praeglacialis en el yacimiento pleistoceno de la sierra de Quibas (Murcia, España). *Estudios Geológicos* **62**: 395–400.

Carlos-Calero JA, Made J van der, Mancheño MA, Montoya P, Romero G. 2006b. *Capra alba* Moyà-Solà, 1987 del Pleistoceno inferior de la Sierra de Quibas (Murcia, España). *Estudios Geológicos* **62**: 571–578.

Chaimanee Y. 1998. Plio-Pleistocene rodents of Thailand. *Thai Studies in Biodiversity* **3**, 1–303.

Channell JE, Singer BS, Jicha BR. 2020. Timing of Quaternary geomagnetic reversals and excursions in volcanic and sedimentary archives. *Quaternary Science Reviews* **228**, 106–114.

Clark TR, Zhao J-x, Roff G, Feng Y-X, Done TJ, Nothdurft LD, Pandolfi JM. 2014. Discerning the timing and cause of historical mortality events in modern Porites from the Great Barrier Reef. *Geochimica Et Cosmochimica Acta* **138**: 57–80.

Colombero S, Carnevale G. 2016. Late Miocene (Turolian, MN13) squirrels from Moncucco Torinese, NW Italy. *Comptes Rendus Palevol* **15**: 515–526.

Colombero S, Pavia G, Carnevale G. 2014. Messinian rodents from Moncucco Torinese, NW Italy: palaeobiodiversity and biochronology. *Geodiversitas* **36**: 421–475.

Cuenca-Bescós G. 1988. Revisión de los Sciuridae del Aragoniense y del Rambliense en la fosa de Calatayud-Montalbán. *Scripta Geologica* **87**: 1–116.

Cuenca-Bescós G, Rofes J, López-García JM, Blain H-A, De Marfá RJ, Galindo-Pellicena MA, Bennásar-Serra ML, Melero-Rubio M, Arsuaga JL, Bermúdez de Castro

JM, Carbonell E. 2010. Biochronology of Spanish Quaternary small vertebrate faunas. *Quaternary International* **212**: 109–119.

Cuenca-Bescós G, Blain H-A, Rofes J, Lozano-Fernández I, López-García JM, Duval M., Galán J, Núnez-Lahuerta C. 2015. Comparing two different Early Pleistocene microfaunal sequences from the caves of Atapuerca, Sima del Elefante and Gran Dolina (Spain): biochronological implications and significance of the Jaramillo subchron. *Quaternary International* **389**: 148–158.

Daams, R. 1981. The dental pattern of the dormice *Dryomys*, *Myomimus*, *Microdyromys* and *Peridyromys*. *Utrech Micropaleontological Bulletin, Special publication* **3**: 1–115.

De Marfà R. 2008. *Oryctolagus giberti* n. sp. (Lagomorpha, Mammalia) du Pléistocène inférieur de Cueva Victoria (Murcie, Espagne). *Comptes Rendus Palévol* **7**: 305–313.

Dietz C, Nill D, Helversen O von. 2009. *Handbook of the Bats of Europe and Northwest Africa*. A&C Black Publishers, Ltd.

Durán JJ, López-Martínez J, Mancheño MA. 2004. Dos registros de espeleotemas pleistocenos de gran potencia en la Península Ibérica: primeros resultados isotópicos. *Boletín Geológico y Minero* **115**: 265–270.

Duval M, Grün R. 2016. Are published ESR dose assessments on fossil tooth enamel reliable? *Quaternary Geochronology* **31**: 19–27.

Duval M, Falguères C, Bahain J-J, Grün R, Shao Q, Aubert M, Dolo J-M, Agustí J, Martínez-Navarro B, Palmqvist P, Toro-Moyano I. 2012a. On the limits of using combined U-series/ESR method to date fossil teeth from two Early Pleistocene archaeological sites of the Orce area (Guadix-Baza basin, Spain). *Quaternary Research* **77**: 482–491.

1104 Duval M, Falguères C, Bahain JJ. 2012b. Age of the oldest hominin settlements in Spain:
1105 Contribution of the combined U-series/ESR dating method applied to fossil teeth.
1106 *Quaternary Geochronology* **10**: 412–417.

1107 Duval M, Fang F, Suraprasit K, Jaeger JJ, Benammi M, Yaowalak C, Iglesias Cibanal J,
1108 Grün R. 2019. Direct ESR dating of the Pleistocene vertebrate assemblage from Khok
1109 Sung locality, Nakhon Ratchasima Province, Northeast Thailand. *Palaeontologia*
1110 *Electronica* **22.3.69**: 1–25.

1111 Duval M, Sahnouni M, Parés JM, van der Made J, Abdessadok S, Harichane Z, Chelli
1112 Cheheb R, Boulaghraif K, Pérez-González A. 2021. The Plio-Pleistocene sequence of
1113 Oued Boucherit (Algeria): a unique chronologically-constrained archaeological and
1114 paleontological record in North Africa. *Quaternary Science Reviews* **271**: 107–116.

1115 Duval M, Arnold LJ, Demuro M, Parés JM, Campaña I, Carbonell E, Bermúdez de Castro
1116 JM (submitted). New chronological constraints for the Early Pleistocene deposits of
1117 Atapuerca Gran Dolina TD1 (Burgos, N Spain). *Quaternary Geochronology*.

1118 Freudenthal M. 2004. Gliridae (Rodentia, Mammalia) from the Eocene and Oligocene of
1119 the Sierra Palomera (Teruel, Spain). *Treballs del Museu de Geologia de Barcelona* **12**:
1120 97–173.

1121 Furió M. 2007. *Los Insectívoros (Soricomorpha, Erinaceomorpha, Mammalia) del*
1122 *Neógeno superior del Levante Ibérico*. PhD Thesis, Universitat Autònoma de Barcelona,
1123 299 pp.

1124 Furió M, Gibert L, Ferràndez C, Sevilla P. 2015. The insectivores (Soricidae, Erinaceidae;
1125 Eulipotyphla; Mammalia) from Cueva Victoria (Early Pleistocene, Murcia, Spain). *Neues*
1126 *Jahrbuch für Geologie und Paläontologie Abhandlungen* **275**: 151–161.

1127 Furió M, van den Hoek Ostende LW, Agustí J, Minwer-Barakat R. 2018. Evolución de
1128 las asociaciones de insectívoros (Eulipotyphla, Mammalia) en España y su relación con
1129 los cambios climáticos del Neógeno y el Cuaternario. *Ecosistemas* **27**: 38–51.

1130 García-Alix A, Minwer-Barakat R, Martín-Suárez E, Freudenthal M. 2009a. Small
1131 mammals from the Early Pleistocene of the Granada Basin, southern Spain. *Quaternary*
1132 *Research* **72**: 265–274.

1133 García-Alix A, Minwer-Barakat R, Martín JM, Martín-Suárez E, Freudenthal M. 2009b.
1134 Dating the change from endorheic to exorheic conditions in the drainage system of the
1135 Granada Basin. *Palaios* **24**: 544–549.

1136 Gibert L, Scott G, Ferràndez-Cañadell C. 2006. — Evaluation of the Olduvai subchron
1137 in the Orce ravine (SE Spain). Implications for Plio-Pleistocene mammal biostratigraphy
1138 and the age of Orce archeological sites. *Quaternary Science Reviews* **25**: 507–525.

1139 Gibert L, Scott GR, Scholz D, Budsky A, Ferrandez C, Ribot F, Martin RA, Lería M.
1140 2016. Chronology for the Cueva Victoria fossil site (SE Spain): evidence for early
1141 Pleistocene Afro-Iberian dispersals. *Journal of Human Evolution* **90**: 183–197.

1142 Gradstein FM, Ogg JG, Schmitz MD, Ogg G. 2012. *The Geologic Time Scale*, p. 1144
1143 (Elsevier, Amsterdam, 2012).

1144 Grün R. 2000a. Methods of dose determination using ESR spectra of tooth enamel.
1145 *Radiation Measurements* **32**: 767–772.

1146 Grün R. 2000b. An alternative model for open system U-series/ESR age calculations:
1147 (closed system U-series)-ESR, CSUS-ESR. *Ancient TL* **18**: 1–4.

1148 Grün R. 2009. The DATA program for the calculation of ESR age estimates on tooth
1149 enamel. *Quaternary Geochronology* **4**: 231–232.

1150 Grün R, Brumby S. 1994. The assessment of errors in past radiation doses extrapolated
1151 from ESR/TL dose-response data. *Radiation Measurements* **23**: 307–315.

1152 Grün R, Katzenberger-Apel O. 1994. An alpha irradiator for ESR dating. *Ancient TL* **12**:
1153 35–38.

1154 Grün R, Schwarcz HP, Chadam J. 1988. ESR dating of tooth enamel: Coupled correction
1155 for U-uptake and U-series disequilibrium. International Journal of Radiation Applications
1156 and Instrumentation. Part D. *Nuclear Tracks and Radiation Measurements* **14**: 237–241.

1157 Guérin G, Mercier N, Adamiec G. 2011. Dose-rate conversion factors: update. *Ancient*
1158 *TL* **29**: 5–8.

1159 Guillén Castejón J. 2010. Canal Negre I, un jaciment càrstic de vertebrats del Miocè,
1160 Pliocè i Pleistocè de Catalunya. *Exploracions* **19**: 7–88.

1161 Guillén Castejón J. 2015. Canal Negre 7: fauna i flora rissianes de final del Pleistocè
1162 Mitjà en el Massís del Garraf (Catalunya). *Exploracions* **21**:11–55.

1163 Gunnell GF, Eiting TP, Geraads D. 2011. New Late Pliocene bats (Chiroptera) from Ahl
1164 al Oughlam, Morocco. *Neues Jahrbuch für Geologie und Paläontologie Abhandlungen*
1165 **260**: 55–71.

1166 Head MJ, Gibbard PL. 2015. Early–Middle Pleistocene transitions: linking terrestrial and
1167 marine realms. *Quaternary International* **389**: 7–46.

1168 Hinton MAC. 1914. On some Remains of Rodents from the Red Crag of Suffolk and from
1169 the Norfolk Forest-Bed. *Annals and Magazine of Natural History* **13**:186–195.

López-García JM, Horacek I, Sevilla P. 2011. *The Contribution of Fossils to the reconstruction of Bat Population Dynamics*. In: Zupan JL, Malakar SL (Eds.), Bats: Biology, Behaviour and Conservation. Nova Science Publishers, Inc.

López-Jiménez A, Haber Uriarte M, López Martínez M, Walker MJ. 2020. Small-mammal indicators of biochronology at Cueva Negra del Estrecho del Río Quípar (Caravaca de la Cruz, Murcia, SE Spain). *Historical Biology* **32**: 18–33.

López-Martínez N. 1989. Revisión sistemática de los Lagomorpha (Mammalia) del Terciario y Cuaternario de España. *Memorias del Museo Paleontológico de la Universidad de Zaragoza* **3**: 1–344.

López-Martínez N, Likius A, Mackaye HT, Vignaud P, Brunet M. 2007. A new lagomorph from the Late Miocene of Chad (Central Africa). *Spanish Journal of Palaeontology* **22**: 1–20.

Lozano-Fernández I, Blain H-A, López-García JM, Agustí J. 2015. Biochronology of the first hominid remains in Europe using the vole *Mimomys savini*: Fuente Nueva 3 and Barranco León D, Guadix-Baza Basin, south-eastern Spain. *Historical Biology* **27**: 1021–1028.

Ludwig K. 2012. Isoplot/Ex, v. 3.75, A Geochronological Toolkit for Microsoft Excel. *Berkeley Geochronology Center Special Publication* **5**: 1–75.

Made van der J, Carlos-Calero JA, Mancheño MA. 2007. New material of the goat *Capra alba* from the Lower Pleistocene of Quibas and Huéscar (Spain). Notes on sexual dimorphism, stratigraphic distribution and systematic. *Bollettino della Societa Paleontologica Italiana* **47**: 13–23.

Madurell-Malapeira J, Minwer-Barakat R, Alba DM, Garcés M, Gómez M, Aurell-

1193 Garrido J, Ros-Montoya S, Moyà-Solà S, Berástegui X. 2010. The Vallparadís section
1194 (Terrassa, Iberian Peninsula) and the latest Villafranchian faunas of Europe. *Quaternary*
1195 *Science Reviews* **29**: 3972–3982.

1196 Marchetti M, Parolin K, Sala B. 2000. The Biharian fauna from Monte La Mesa (Verona,
1197 northeastern Italy). *Acta Zoologica Cracoviensia* **43**: 79–105.

1198 Marsh RE. 1999. *Beta-gradient Isochrons Using Electron Paramagnetic Resonance:*
1199 *Towards a New Dating Method in Archaeology*. MSc thesis, McMaster University.

1200 Martín-Suárez E, Mein P. 1991. Revision of the genus *Castillomys* (Muridae, Rodentia).
1201 *Scripta Geologica* **96**: 47–81.

1202 Martín-Suárez E, Mein P. 1998. Revision of the genera *Parapodemus*, *Apodemus*,
1203 *Rhagamys* and *Rhagapodemus* (Rodentia, Mammalia). *Geobios* **31**: 87–97.

1204 Martín-Suárez E, Freudenthal M. 1993. Muridae (Rodentia) from the lower Turolian of
1205 Crevillente (Alicante, Spain). *Scripta Geologica* **103**: 65–118.

1206 Mein P, Moissenet E, Truc G. 1978. Les formations continentales du Néogene supérieur
1207 des vallées du Júcar et du et du Cabriel au NE d'Albacete (Espagne). Biostratigraphie et
1208 environnements. *Documents des Laboratoires de Géologie de la Faculté des Sciences de*
1209 *Lyon* **72**: 99–137.

1210 Meulen A Van Der. 1973. Middle Pleistocene smaller mammals from the Monte Peglia,
1211 (Orvieto, Italy) with special reference to the phylogeny of *Microtus* (Arvicolidae, Rodentia).
1212 *Quaternaria* **17**: 1–114.

1213 Minwer-Barakat R, García-Alix A, Martín-Suárez E, Freudenthal M. 2005. Muridae
1214 (Rodentia) from the Pliocene of Tollo de Chiclana (Granada, southeastern Spain). *Journal*

of Vertebrate Paleontology **25**: 426–441.

Minwer-Barakat R., Madurell-Malapeira J, Alba DM, Aurell-Garrido J, De Esteban-Trivigno S, Moyà-Solà S. 2011. Pleistocene rodents from the Torrent de Vallparadís section (Terrassa, northeastern Spain) and biochronological implications. *Journal of Vertebrate Paleontology* **31**: 849–865.

Montoya P, Alberdi MT, Blázquez AM, Barbadillo LJ, Fumanal MP, Made van der J, Marín JM, Molina A, Morales J, Murelaga X, Peñalver E, Robles F, Ruiz Bustos A, Sánchez A, Sanchiz B, Soria D, Szyndlar Z. 1999. La fauna del Pleistoceno inferior de la Sierra de Quibas (Abanilla, Murcia). *Estudios Geológicos* **55**: 127–161.

Montoya P, Alberdi MT, Barbadillo LJ, Made van der J, Morales J, Murelaga X, Peñalver E, Robles F, Ruiz Bustos A., Sánchez A, Sanchiz B, Soria S, Szyndlar Z. 2001. Une faune très diversifiée du Pléistocène inférieur de la Sierra de Quibas (provincia de Murcia, Espagne). *Comptes Rendus de l'Académie des Sciences, Series IIa* **332**: 387–393.

Muttoni G, Scardia G, Kent DV. 2010. Human migration into Europe during the late Early Pleistocene climate transition. *Palaeogeography, Palaeoclimatology, Palaeoecology* **296**: 79–93.

Oms O, Garcés M, Parés JM, Agustí J., Anadón P, Julià R. 1994. Magnetostratigraphic characterization of a thick Lower Pleistocene lacustrine sequence from the Baza basin (Betic chain, southern Spain). *Physics of the Earth and Planetary Interiors* **85**: 173–180.

Oms O, Agustí J, Gabas M, Anadón P. 2000a. Lithostratigraphical correlation of micromammal sites and biostratigraphy of the Upper Pliocene to Lower Pleistocene in the Northeast Guadix- Baza Basin (Southern Spain). *Journal of Quaternary Science* **15**: 43–50.

1238 Oms O, Parés JM, Martínez-Navarro B, Agustí J, Toro I, Martínez-Fernández G, Turq A.
1239 2000b. Early human occupation of Western Europe: paleomagnetic dates for two
1240 paleolithic sites in Spain. *Proceedings of the National Academy of Sciences* **97**: 10666–
1241 10670.

1242 Oms O, Anadón P, Agustí J, Julià R. 2011. Geology and chronology of the continental
1243 Pleistocene archeological and paleontological sites of the Orce area (Baza basin, Spain).
1244 *Quaternary International* **243**: 33–43.

1245 Parés JM, Álvarez C, Sier M, Moreno D, Duval M, Woodhead JD, Ortega AI, Campaña
1246 I, Rosell J, Bermúdez de Castro JM, Carbonell E. 2018. Chronology of the cave interior
1247 sediments at Gran Dolina archaeological site, Atapuerca (Spain). *Quaternary Science*
1248 *Reviews* **186**: 1–16.

1249 Parés JM, Pérez-González A. 1999. Magnetochronology and stratigraphy at gran Dolina
1250 section, Atapuerca (Burgos, Spain). *Journal of Human Evolution* **37**: 325–342.

1251 Pelletier M, Cochard D, Boudadi-Maligne M, Crochet J-Y, Bourguignon L. 2015. Lower
1252 Pleistocene leporids (Lagomorpha, Mammalia) in Western Europe: New data from the
1253 Bois-de-Riquet (Lézignan-la-Cèbe, Hérault, France). *Comptes Rendus Palevol* **14**: 371–
1254 385.

1255 Pérez-García A, Murelaga X, Mancheño MA, Rodríguez AA, Romero G. 2015. The
1256 tortoises from the Lower Pleistocene palaeontological site of Quibas (Region de Murcia,
1257 Spain). *Comptes Rendus Palevol* **14**: 589–603.

1258 Piñero P, Agustí J. 2019. The rodent succession in the Sifón de Librilla section (Fortuna
1259 Basin, SE Spain): implications for the Mio-Pliocene boundary in the Mediterranean
1260 terrestrial record. *Historical Biology* **31**: 279–321.

1261 Piñero P, Alberdi MT. 2015. Estudio de los caballos del yacimiento de Quibas,
1262 Pleistoceno Inferior final (Abanilla, Murcia, España). *Estudios Geológicos* **71**: e034.

1263 Piñero P, Agustí J, Blain H-A, Furió M, Laplana C. 2015. Biochronological data for the
1264 Early Pleistocene site of Quibas (SE Spain) inferred from rodent assemblage. *Geologica*
1265 *Acta* **13**: 229–241.

1266 Piñero P, Agustí J, Blain H-A, Laplana C. 2016. Paleoenvironmental reconstruction of
1267 the Early Pleistocene site of Quibas (SE Spain) using a rodent assemblage. *Comptes*
1268 *Rendus Palevol* **15**: 659–668.

1269 Piñero P, Agustí J, Oms O, Blain H-A, Furió M, Laplana C, Sevilla P, Rosas A, Vallverdú
1270 J. 2020. First continuous pre-Jaramillo to Jaramillo terrestrial vertebrate succession from
1271 Europe. *Scientific Reports* **10**: 1–11.

1272 Prescott JR, Hutton JT. 1994. Cosmic ray contributions to dose rates for luminescence
1273 and ESR dating: large depths and long-term time variations. *Radiation measurements* **23**:
1274 497–500.

1275 Rodríguez J, Burjachs F, Cuenca-Bescós G, García N, Van der Made J, Pérez González
1276 A, Blain H-A, Expósito I, López-García JM, García Antón M, Allué E, Cáceres I, Huguet
1277 R, Mosquera M, Ollé A, Rosell J, Parés JM, Rodríguez XP, Díez C, Rofes J, Sala R,
1278 Saladié P, Vallverdú P, Bennasar ML, Blasco R, Bermúdez de Castro JM, Carbonell E.
1279 2011. One million years of cultural evolution in a stable environment at Atapuerca
1280 (Burgos, Spain). *Quaternary Science Reviews* **30**: 1396–1412.

1281 Reumer JWF. 1984. Ruscinian and early Pleistocene Soricidae (Insectivora, Mammalia)
1282 from Tegelen (The Netherlands) and Hungary. *Scripta Geologica* **73**: 1–173.

1283 Reumer JWF, van der Hoek Ostende LW. 2003. Petauristidae and Sciuridae (Mammalia,
1284 Rodentia) from Tegelen, Zuurland, and the Maasvlakte (the Netherlands). *Deinsea* **10**:
1285 455–467.

1286 Rodríguez-Estrella T, Mancheño MA, Romero G, Hernández JM. 2004. Características
1287 geológicas de la Sierra de Quibas (Abanilla, Murcia). Su relación con un yacimiento
1288 paleontológico pleistoceno. *Geogaceta* **35**: 115–118.

1289 Rofes J, Cuenca-Bescós G. 2006. First evidence of the Soricidae (Mammalia) *Asoriculus*
1290 *gibberodon* (Petényi, 1864) in the Pleistocene of North Iberia. *Rivista Italiana di*
1291 *Paleontologia e Stratigrafia* **112**: 301–315.

1292 Rofes J, Cuenca-Bescós G. 2011. Evolutionary history and biogeography of the genus
1293 *Crocidura* (Mammalia, Soricidae) in Europe, with emphasis on *Crocidura kornfeldi*.
1294 *Mammalian Biology* **76**: 64–78.

1295 Rzebik-Kowalska B. 2013. *Sorex bifidus* n. sp. and the rich insectivore mammal fauna
1296 (Erinaceomorpha, Soricomorpha, Mammalia) from the Early Pleistocene of Żabia Cave
1297 in Poland. *Palaeontologia Electronica* **16.2.12**: 1–35.

1298 Sala B, Masini F. 2007. Late Pliocene and Pleistocene small mammal chronology in the
1299 Italian peninsula. *Quaternary International* **160**: 4–16.

1300 Scott GR, Gibert L, Gibert J. 2007. Magnetostratigraphy of the Orce region (Baza Basin),
1301 SE Spain: New chronologies for Early Pleistocene faunas and hominid occupation sites.
1302 *Quaternary Science Reviews* **26**: 415–435.

1303 Sevilla P. 1988. Estudio paleontológico de los Quirópteros del Cuaternario español.
1304 *Paleontologia i Evolució* **22**: 113–233.

Sevilla P. 1991. *Murciélagos fósiles de España*. In: Benzal J, Paz O de (Eds.), Los Murciélagos de España y Portugal. Monografías del ICONA, Colección Técnica. Madrid, p. 21–36.

Sevilla P. 2012. The Lower Pleistocene Bats from Cueva Victoria. *Revista del Museo Arqueológico Municipal de Cartagena* **11–13**: 239–252.

Sevilla P, Furió M. 2010. *The Plio-Pleistocene bat fossils of the Almenara-Casablanca Complex: getting closer to a modern assemblage*. 15th International Bat Research Congress. Abstracts Book. Prague, p. 283.

Sevilla P, López-García JM. 2010. *The Quaternary fossil record of Bats in Spain: an update*. In: Horacek I, Benda P (Eds.), 15th International Bat Research Symposium. Prague 2010, p. 284.

Sevilla P, Agustí J, Blain H-A, Laplana C, Romero G, Mancheño MA. 2014. *Los murciélagos del Pleistoceno inferior de Quibas (Abanilla, Murcia, España)*. In: Royo-Torres R, Verdú FJ, Acalá L (Eds.), XXX Jornadas de la Sociedad española de Paleontología. ¡Fundamental! 24, p. 229–231.

Sinitsa MV, Pogodina NV. 2019. The evolution of early *Spermophilus* in eastern Europe and the antiquity of the Old World ground squirrels. *Acta Palaeontologica Polonica* **64**: 643–667.

Sulimski A. 1964. Pliocene Lagomorpha and Rodentia from Weze 1 (Poland). *Acta Palaeontologica Polonica* **9**:149–244.

Thorington RW, Musante AL, Anderson CG, Darrow K. 1996. Validity of three genera of flying squirrels: *Eoglaucomys*, *Glaucomys*, and *Hylopetes*. *Journal of Mammalogy* **77**: 69–83.

1328 Thorington RW, Schennum CE, Pappas LA, Pitassy D. 2005. The difficulties of
1329 identifying flying squirrels (Sciuridae: Pteromyini) in the fossil record. *Journal of*
1330 *Vertebrate Paleontology* **25**: 950–961.

1331 Toro-Moyano I, Martinez-Navarro B, Agustí J, Souday C, Bermúdez de Castro JM,
1332 Martinón-Torres M, Fajardo B, Duval M, Falgueres C, Oms O, Pares JM, Anadón P, Julià
1333 R, García-Aguilar JM, Moigne A-M, Espigares MP, Ros-Montoya S, Palmqvist P. 2013.
1334 The oldest human fossil in Europe, from Orce (Spain). *Journal of Human Evolution* **65**:
1335 1–9.

1336 Van de Weerd A. 1976. Rodent faunas of the Mio-Pliocene continental sediments of the
1337 Teruel-Alfambra region, Spain. *Utrech Micropaleontological Bulletin, Special*
1338 *Publication* **2**: 1–217.

1339 Van den Hoek Ostende LW, Reumer JWF. 2011. *Hylopetes magistri*, New Name for
1340 *Hylopetes debruijni* Reumer & Van den Hoek Ostende, 2003, Preoccupied. *Journal of*
1341 *Vertebrate Paleontology*: **31**: 928–928.

1342 Walker MJ, Haber Uriarte M, López Jiménez A, López Martínez M, Made J van der,
1343 Duval M, Grün R. 2020. Cueva Negra del Estrecho del Río Quípar: A dated Early
1344 Pleistocene Palaeolithic site in southeastern Spain. *Journal of Paleolithic Archaeology* **3**:
1345 816–855.

1346 Zhao JX, Hu K, Collerson KD, Xu HK. 2001. Thermal ionization mass spectrometry U-
1347 series dating of a hominid site near Nanjing, China. *Geology* **29**: 27–30.

1348

Tables

Table 1. ESR fitting results obtained for sample #595. Intensity precision is expressed as the mean coefficient of variation of the ESR intensities obtained for all the aliquots of a given sample over the three repeated measurements. D_E precision is the variation of the D_E values (1 relative standard deviation) derived from each repeated measurements of a given sample. D_{max} corresponds to the maximum irradiation dose considered for the fitting. Given the magnitude of the D_E values, D_{max}/D_E ratio should be between 5 and 10 according to Duval and Grün (2016).

Sample	**#595**
Average weight per aliquot (mg)	20.1 ± 0.2
Number of repeated measurements	3
Measurement precision (%)	1.5
SSE fitting (data weighting by $1/I^2$)	
D_E precision (%)	3.8
Adj. r-Square	0.996
D_{E1} (Gy)	1835 ± 143
D_{max} (Gy)	2965
D_{max}/D_E	1.6
SSE fitting (data weighting by $1/s^2$)	
Adj. r-Square	0.996
D_{E5} (Gy)	1720 ± 146
D_{max} (Gy)	2965
D_{max}/D_{E2}	1.7
D_E ratios	

D_{E2}/D_{E1} ratio	0.94

Table 2. Data inputs and outputs corresponding to the combined US-ESR age calculations for the tooth samples from Quibas-Sima. All errors are given at a 1-σ confidence level, with the exception of the U-series ages (2-σ; marked by (1)). Final D_E errors are made of a combination of errors from the fitting (Table 1) and the dose rate from the gamma source (2.3%). Post-Rn equilibrium was considered in dental tissues and sediment. Corrected U-series age are calculated by applying non-radiogenic ^{230}Th correction, assuming non-radiogenic $^{230}Th/^{232}Th$ = 0.825+/-50% (bulk-Earth value), with ^{238}U, ^{234}U, ^{232}Th and ^{230}Th in secular equilibrium.

SAMPLE	**#595**
Unit	**QS-3**
Enamel	
Dose (Gy)	1835 ± 149
U (ppm) (1)	5.715 ± 0.005
$^{234}U/^{238}U$ (1)	1.4437 ± 0.0013
$^{230}Th/^{238}U$ (1)	1.4922 ± 0.0028
$^{230}Th/^{232}Th$ (1)	444 ± 8
Corrected U-series age (ka) (1)	269.5 ± 2.3
Initial $^{234}U/^{238}U$ (1)	2.0619 ± 0.0077
Alpha Efficiency	0.13 ± 0.02
Water content (%)	0
Initial enamel thickness (μm)	1267 ± 127
Dentine	

U (ppm) [(1)]	38.821 ± 0.049
$^{234}U/^{238}U$ [(1)]	1.5484 ± 0.0010
$^{230}Th/^{238}U$ [(1)]	1.5650 ± 0.0030
$^{230}Th/^{232}Th$ [(1)]	252 ± 1
Corrected U-series age (ka) [(1)]	309.1 ± 3.0
Initial $^{234}U/^{238}U$ [(1)]	2.1792 ± 0.0065
Water (%)	5 ± 3
Removed enamel thickness (μm)	213 ± 21
Sediment	
U (ppm)	1.35 ± 0.08
Th (ppm)	4.01 ± 0.17
K (%)	0.61 ± 0.02
Water (wet % weight)	20 ± 5
Removed thickness (μm)	232 ± 23
Combined U-series/ESR age calculations	
internal dose rate (μGy a^{-1})	3557 ± 1212
beta dose rate, dentine (μGy a^{-1})	868 ± 422
beta dose rate, sediment (μGy a^{-1})	44 ± 6
Gamma + cosmic dose rate (μGy a^{-1})	493 ± 30
Total dose rate (μGy a^{-1})	4962 ± 1283
p enamel	-0.95
p dentine	-1
US-ESR age (ka)	369 +28 -53
CSUS-ESR age (ka)	1431 ± 278

1366

Table 3. Percentage of each morphotype in the M1s of *Apodemus sylvaticus* from each level in the Quibas-Sima sequence. Notes: N = number of elements.

Level	Morphotype 1		Morphotype 2	
	N	%	N	%
QS-1.1	0	0	3	100
QS-1.2	8	24	26	76
QS-1.3	26	40	40	60
QS-2	2	50	2	50
QS-3	6	86	1	14
QS-4	2	67	1	33
QS-7	0	0	1	100